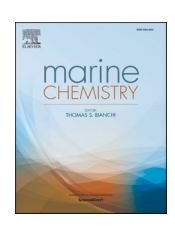
\$ SUPER

Contents lists available at ScienceDirect

# Marine Chemistry

journal homepage: www.elsevier.com/locate/marchem





# Biogenic and lithogenic silicon along the GEOTRACES south West Indian Ocean section (SWINGS-GS02) and the islands mass effect on regional Si biogeochemical cycle

Valentin Deteix <sup>a,\*</sup>, Edwin Cotard <sup>a</sup>, Sandrine Caquineau <sup>a</sup>, William M. Landing <sup>b</sup>, Frédéric Planchon <sup>c</sup>, Thomas Ryan-Keogh <sup>d</sup>, Damien Cardinal <sup>a</sup>

- <sup>a</sup> LOCEAN-IPSL, Laboratoire d'Océanographie et du Climat : Expérimentations et Approches Numériques, UMR 7159 (Sorbonne Université-CNRS-MNHN-IRD), 4 Place Jussieu, 75005 Paris, France
- b Department of Earth, Ocean and Atmospheric Science, Florida State University, 1011 Academic Way, Tallahassee, FL, USA
- <sup>c</sup> LEMAR, Laboratoire des Sciences de l'Environnement Marin, UMR 6539 (Université de Bretagne Occidentale-CNRS-IRD-Ifremer), Rue Dumont d'Urville, 29280 Plouzané, France
- d Southern Ocean Carbon-Climate Observatory, CSIR, Cape Town, South Africa

#### ARTICLE INFO

#### Keywords: Biogenic and lithogenic silicon GEOTRACES Southern Ocean Scanning electron microscopy

#### ABSTRACT

The distribution and cycling of biogenic silica (BSi) and lithogenic silicon (LSi) in the ocean play crucial roles in the global silicon cycle and marine ecosystem dynamics. This is especially the case in the Southern Ocean where diatoms constitute the predominant phytoplankton and participate in a major way to the biological carbon pump. This study presents an assessment of BSi and LSi concentrations along the GEOTRACES South West Indian Ocean Section (SWINGS, late austral summer 2021), where several and contrasting regions were encountered: oligotrophic Mozambique basin, HNLC (High Nutrient Low Chlorophyll) areas and regions fertilized by the Subantarctic islands, Suspended particles were sampled from Niskin bottles and in situ pumps, along with scanning electron microscope (SEM) observations and specific pigments measurements to support BSi and LSi analyses. With samples coming from a contrasting study area prone to diverse continental influences, our BSi and LSi results showed a reproducibility of  $13 \pm 7\%$ , in the same range as the established protocol. BSi concentrations show a north-south gradient with maxima encountered in the Antarctic Zone, and contrasted results between HNLC open ocean areas and naturally fertilized regions in the vicinity of the Subantarctic islands. Some open ocean stations have unusually high BSi (e.g.  $> 5 \mu \text{mol L}^{-1}$ ) likely resulting from fertilization by aerosols, upwelling or island mass effect when they are downstream of the islands. Coupling of BSi with SEM observations and pigments measurements respectively showed diatoms were the most representative of the carrying phase of BSi and suggested silicification changes, induced either by heavily silicified diatoms or by micronutrient limitation in HNLC regions. BSi is often dominated by the smallest size fraction (0.45–5  $\mu m$ ) which represent 47  $\pm$ 23% of the total BSi based on 29 measurements on size fractionated samples. LSi results highlighted atmospheric inputs at the surface and nepheloid layers in the water column, which makes LSi overall a good indicator of the origin of lithogenic materials. SEM observations supported these results, enabling characterization of the diversity of lithogenic materials in the vicinity of the Subantarctic islands, more specifically volcanic ash around Heard Island, and within the nepheloid layers.

#### 1. Introduction

Silicon (Si) constitutes the most abundant element by mass at the Earth's surface after oxygen, and is a key nutrient for some aquatic organisms. The marine biogeochemical Si cycle is controlled by fluxes

between the dissolved pool ( $< 0.45 \, \mu m$ ), composed almost exclusively of orthosilicic acid Si(OH)<sub>4</sub>, and the particulate pool ( $> 0.45 \, \mu m$ ) (Tréguer et al., 2021). The latter consists of two components: biogenic silica (BSi) in the form of opal (amorphous SiO<sub>2</sub> nH<sub>2</sub>O), a product of silicification by marine organisms such as siliceous plankton, and lithogenic silicon

E-mail address: valentin.deteix@locean.ipsl.fr (V. Deteix).

<sup>\*</sup> Corresponding author.

(LSi), which is comprised of non-biogenic minerals containing Si, silicates being the main mineral group and making up the bulk of rocks in the Earth's crust.

The South Indian Ocean is a unique oceanic region composed of contrasting biogeochemical provinces including its austral region in the Southern Ocean. The latter is characterised by a relatively low phytoplanktonic primary productivity, despite the latitudinal gradient of macronutrients increasing southward. This paradox is mainly due to a lack of micronutrients in the surface waters such as iron (Fe) or manganese (Mn) (Martin, 1990), but other co-limitations are also present, such as light availability as well as macronutrients (Nelson and W. 0. Smith Jr., 1991; Sedwick et al., 2002). The Subtropical zone (STZ), located north of the subtropical front (STF) in the oligotrophic subtropical gyre, has Low Nutrient Low Chlorophyll (LNLC) conditions where "nutrient" refers to macronutrients:  $NO_x$  ( $NO_3^- + NO_2^-$ ), dissolved inorganic phosphorus (DIP) and Si(OH)<sub>4</sub>. The Subantarctic zone (SAZ), between the STF and the subantarctic front (SAF), and the Polar Frontal zone (PFZ), between the SAF and the polar front (PF), display both relatively high NO<sub>x</sub> and DIP concentrations in the surface waters, yet Si  $(OH)_4$  concentrations remain low (i.e. often  $<5 \mu mol L^{-1}$ ). This results in the characterization of High Nutrient Low Silicon Low Chlorophyll (HN-Low Si-LC) conditions in the SAZ and PFZ (Dugdale et al., 1995; Nelson et al., 2001). Finally, the Antarctic Zone (AZ), located south of the PF, does not have Si(OH)4 limitation due to upwelling occurring at the Antarctic divergence, south of the PF, which is transported northward by Ekman surface transport on multiannual timescales (Sarmiento et al., 2004), but also by seasonal mixing in the subsurface. The AZ is thus characterised by High Nutrient Low Chlorophyll (HNLC) conditions (Nissen et al., 2021). BSi exported to deep waters is remineralized, yet less quickly than organic matter, leading to a Si(OH)<sub>4</sub> trapping in the deep waters (Holzer et al., 2014), which explains the stronger gradient of decreasing surface Si(OH)<sub>4</sub> concentrations relative to NO<sub>3</sub> (Sarmiento et al., 2004).

Despite this relatively low chlorophyll content, the Southern Ocean plays a crucial role in global climate regulation, by contributing significantly to global primary production as well as to bottom water, intermediate water and mode water formation, which makes it a major carbon sink (Gruber et al., 2019). A minor though significant part of this carbon sink is due to the biological carbon pump, i.e. the transfer of the organic carbon biologically fixed by primary production, from the euphotic zone into the deep ocean through several processes, including the export of particulate organic carbon (POC) associated with particle settling (Le Moigne, 2019). Although the biological carbon pump has received significant attention, the magnitude of this process remains poorly quantified, from 5 to 13 PgC yr<sup>-1</sup> depending on the constraints applied in biogeochemical models (Henson et al., 2011; Siegel et al., 2014; DeVries and Weber, 2017; Clements et al., 2023). In the Southern Ocean, diatoms, a phytoplanktonic group that produces opal cell skeleton called frustules, play a key role in the biological carbon pump and thus in global climate regulation. Contributing up to 40% of the total primary production in the global oceans (Field et al., 1998), diatoms control most of POC and BSi export, with a global opal pelagic production of 255  $\pm$  52 TmolSi yr $^{-1}$ , of which 26% occurs in the Southern Ocean (Tréguer et al., 2021).

Lithogenic silicon (LSi) is often neglected in the global ocean silicon cycle since it is considered as non-dissolvable (e.g. Tréguer et al., 2021). However, it is a good proxy for understanding the origin and transport of lithogenic materials, which can come from continental inputs in the form of aerosols such as dust and volcanic ashes (e.g. Geisen et al., 2022), fluvial or coastal erosion-induced inputs (Regard et al., 2022) and resuspension of sediments in the water column (Quéguiner et al., 1997). In some Southern Ocean areas, lithogenic material including LSi can be a significant source of Si and/or micronutrients and can possibly induce a phytoplanktonic response (Fripiat et al., 2011; van der Merwe et al., 2019; Geisen et al., 2022). Thus, it goes hand in hand with BSi to understand the relations between these two components of the particulate

pool with the marine biogeochemical Si cycle.

The SWINGS (South West Indian GEOTRACES Section) cruise took place during the late austral summer 2021 in the South Indian Ocean including the south Indian sector of the Southern Ocean. The general aim was to elucidate sources, transformations and fate of various biogeochemically important elements, especially trace elements, along a transect covering a large spectrum of biogeochemical provinces. This includes (i) the South African coastal waters, (ii) the offshore waters with LNLC, HN-Low Si-LC and HNLC areas, and (iii) the waters affected by the island mass effect. This process in the study region results whether from natural iron fertilization for the Kerguelen Plateau (Blain et al., 2007) and the Crozet archipelago (Pollard et al., 2009), or from mesoscale eddies and Antarctic Circumpolar Current (ACC) frontal meanders for the Prince Edward Islands (Lamont et al., 2022).

In this paper, we investigated the spatial variability of BSi and LSi concentrations along the SWINGS section, comparing (i) sampling from Niskin bottles and *in situ* pumps, plus (ii) different size fractions. Results were coupled with high performance liquid chromatography (HPLC) pigments analyses and scanning electron microscope observations, to identify carrying phases of BSi and LSi. Finally, we discuss the BSi and LSi calculation methods to illustrate the relevance and limitations of each method.

#### 2. Materials and methods

#### 2.1. Cruise transect - Sampling strategy

The SWINGS cruise was conducted along a transect in the South West Indian Ocean and Southern Ocean sectors, in both offshore waters and waters surrounding several Subantarctic islands, from January 11th to March 8th 2021, on-board R/V "Marion Dufresne II". The sampling covers: oligotrophic Mozambique basin in the STZ, HN-Low Si-LC and HNLC regions in the SAZ, PFZ and AZ (Fig. 1a), and areas in the vicinity of the Subantarctic islands: Marion and Prince Edward Islands (Fig. 1b), naturally iron-fertilized Crozet archipelago (Fig. 1c) and naturally iron-fertilized Kerguelen Plateau, including Heard and MacDonald Islands (Fig. 1d). The study area covers several contrasting biogeochemical provinces and is influenced by important advective features: Agulhas return current, ACC and "Fawn Trough" current (Sokolov and Rintoul, 2009).

For BSi and LSi, 37 stations were sampled, with a total of 473 particulate samples analysed in this study (Fig. 1). This includes 267 total particulate samples collected using Niskin bottles (NSK; > 0.8 µm; 37 stations) and in situ pumps (ISP;  $> 0.45 \mu m$ ; 15 stations), plus 170 sizefractionated samples collected using in situ pumps (ISP-SF; 5–53 µm; > 53 µm; 13 stations). NSK samples were collected using a Rosette equipped with 12 L Niskin bottles, with 3 to 5 depths in the first 200 m plus an additional sample from 500 m depth. Between 1 and 6 L of seawater was immediately filtered on-board through polyethersulfone (PES) membranes (PALL SUPOR®, 47 mm, 0.8 µm pore size) under airfiltered (Nuclepore® polycarbonate membrane, 0.6 µm pore size) pressurised filtration units. Membranes were rinsed with  $\sim \! \! 10$  mL of Milli-Q water (18.2 m $\Omega$ ) using a wash bottle while applying suction, dried for 24 h at 60 °C in plastic Petri dishes and then stored at room temperature. For ISP samples, 90 to 1200 L of seawater was filtered through polyethersulfone membranes (PALL SUPOR®, 142 mm, 0.45 μm pore size) using *in situ* pumps, at 2 to 8 depths along the whole water column. For ISP-SF samples, 40 to 1400 L was filtered through woven mesh membranes generating two size fractions: 5–53 μm (PETEX®, 142 mm, 5  $\mu m$  pore size) and > 53  $\mu m$  (PETEX®, 142 mm, 53  $\mu m$  pore size), at 4 to 8 depths in the first 800 m. After pump recovery, both ISP and ISP-SF filter heads were immediately opened on-board and their membranes were cut for subsampling under a laminar-flow hood in an ultraclean atmosphere, while ISP-SF were cut in a standard laboratory onboard. Approximatively one quarter of those membranes were dedicated to BSi and LSi analysis. For ISP-SF samples, particles were washed from

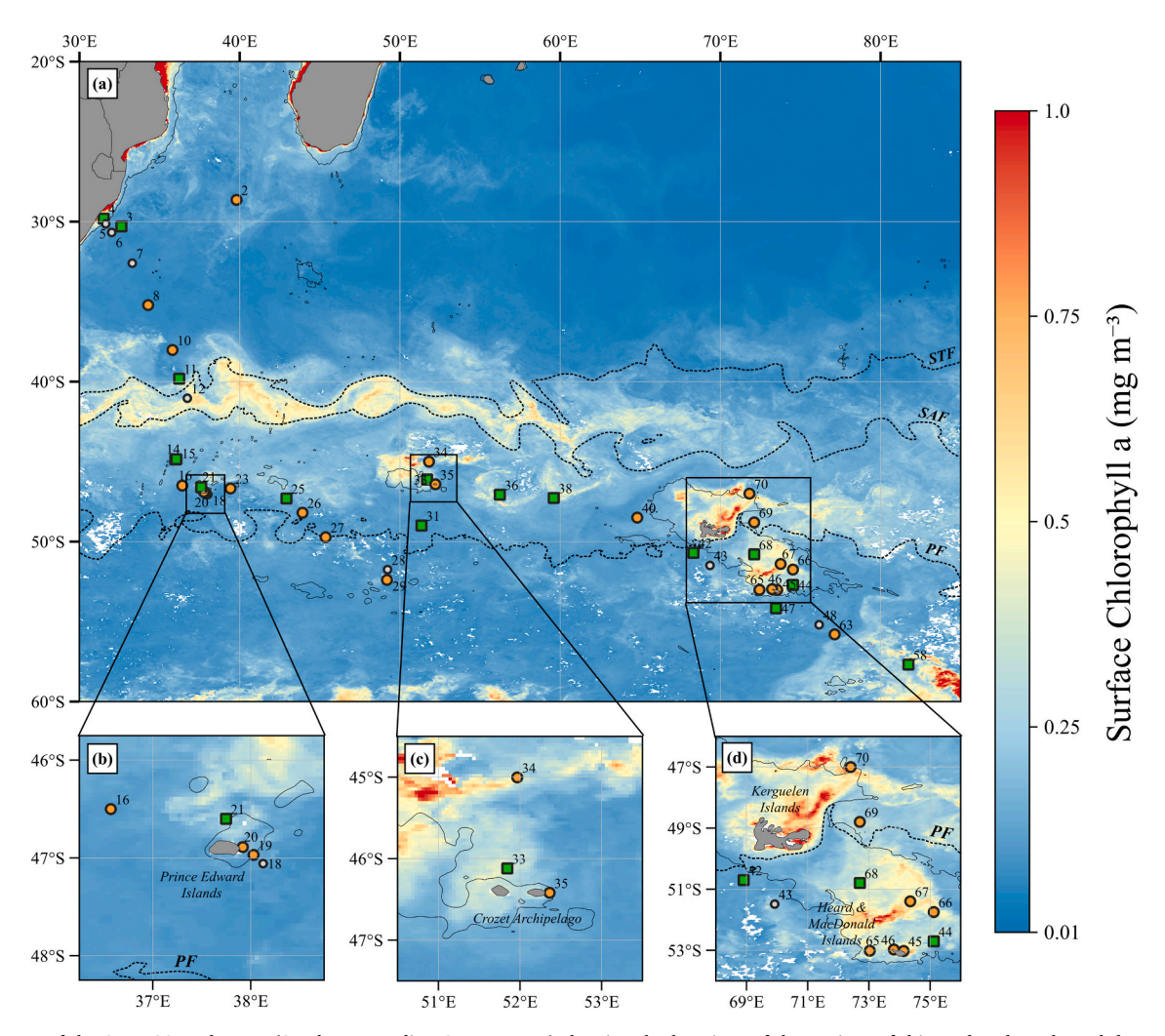


**Fig. 1.** (a) Map of the SWINGS study area (South West Indian Ocean sector) showing the locations of the stations of this study. The coloured dots represent the different station types for sampling: green for *in situ* pump and Niskin bottles, orange for Niskin bottles, grey for pigment sampling only. The colour represents the detailed map of the satellite-derived surface chlorophyll *a* concentration averaged over February 2021 (MODIS L3 product). The black lines represent the 1000 m isobath from GEBCO bathymetry. The dotted lines represent the positions of the Southern Ocean fronts determined from satellite-derived surface temperature averaged over February 2021 (CMEMS L4 product): STF = Subtropical Front (18 °C); SAF = Subantarctic Front (13 °C); PF = Polar Front (4.5 °C). Inset maps show details of the areas of particular interest: (b) Prince Edward islands area; (c) Crozet Archipelago; (d) Kerguelen Plateau.

the cut PETEX membrane with filtered seawater (0.4  $\mu$ m), and resuspended aliquots were filtered through polycarbonate membranes (Nuclepore®, 25 mm, 0.4  $\mu$ m pore size). Both final polyethersulfone (ISP) and polycarbonate (ISP-SF) membranes were dried for 24 h at 60 °C in plastic Petri dishes and then stored at room temperature.

# 2.2. Particle digestion - BSi and LSi analyses

Before particle digestion, membranes were cut in thirds (ISP samples), in half or quarter (ISP-SF samples), and in half (NSK samples). The exact cut portion was determined only for polyethersulfone filters, *i.e.* ISP and NSK samples, with a precision balance (METTLER TOLEDO® AG245, 0.1 mg). Extraction of BSi and LSi was performed under a laminar-flow hood in a clean room, following a protocol adapted from Ragueneau et al. (2005) initially developed for coastal samples (*i.e.* rather concentrated in LSi). Membranes were digested with two identical wet-alkaline leachings using NaOH solution (4 mL, 0.2 M, AnalaR Normapur®) in Teflon tubes at 95 °C for 40 min, followed by neutralization of the reaction with HCl solution (1 mL, 1 M, AnalaR Suprapur®); both Si and aluminium (Al) concentrations were measured in each leach solution (L1 and L2). Such alkaline leaching has been commonly used in the open ocean (Brzezinski and Nelson, 1989, Brzezinski and Nelson,

1995), including the Southern Ocean (Franck et al., 2000). After the double alkaline digestion, a third acidic digestion (48 h at room temperature) was performed using HF solution (0.5 mL, 2.9 M, AnalaR Suprapur®) on dried filters, where only Si concentrations are measured (L3). Al concentrations in the alkaline digestions are used as an indicator of LSi dissolution, enabling the correction and quantification of BSi measurements using a sample specific Si:Al ratio (Ragueneau et al., 2005; see section 2.3) as follows:

$$[BSi] = [Si]_1 - [Al]_1 * ([Si] : [Al])_2.$$
(1)

$$[LSi] = [Si]_3 + [Si]_2 + ([Si]_1 - [BSi]).$$
(2)

where subscripts refer to # of leaching.

Si<sub>1</sub> and Si<sub>2</sub> concentrations were determined by spectrophotometry (ThermoScientific® Evolution 220) following the colorimetric silicomolybdic acid method described by Grasshoff et al. (2009). Accuracy was checked with certified reference material (fluvial freshwater Perade-09, National Research Council Canada:  $110.02 \pm 6.98 \, \mu \text{mol L}^{-1}$ ) and secondary reference material that was intercalibrated for Si(OH)<sub>4</sub> (fluvial freshwater SLRS-6, National Research Council Canada:  $79.43 \pm 4.55 \, \mu \text{mol L}^{-1}$ ; Yeghicheyan et al., 2019). For the third leaching, as the presence of HF affects the absorbance of the solution above a 0.05%

concentration (=  $0.025~\mu mol~L^{-1}$ , Eggimann and Betzer, 1976), samples have been diluted by a factor of 150 with a supersaturated boric acid solution (AnalaR Normapur®), to remain below this threshold and increase the sensitivity of LSi measurements (Brzezinski and Nelson, 1995). Al concentrations were determined using an ICP-QMS (Inductively Coupled Plasma-Quadrupole Mass Spectrometry, Agilent® 7900) at the PARI analytical platform (Institut de Physique du Globe de Paris, IPGP, Paris, France) using a He collision cell, with scandium and indium as internal standards to correct the instrument drift. Accuracy was checked with certified reference material (fluvial freshwater SLRS-6, National Research Council Canada:  $33.9 \pm 2.2~ppb$ ).

Blank measurements were performed by applying the same protocol. For ISP blanks (n = 10), membranes were placed on *in situ* pumps but no seawater was pumped when deployed at sea (i.e. corresponds to "dipped" blanks). For ISP-SF blanks (n = 3), 100 mL of Milli-Q water was filtered on-board. For NSK blanks (n = 10), approximatively 2 L of Milli-Q water was filtered on-board. Blank values for Si in the first leaching (Si<sub>1</sub>) were 47.0  $\pm$  36.6 nmol for ISP, 22.8  $\pm$  17.0 nmol for ISP-SF and  $30.6 \pm 26.9$  nmol for NSK. The detection limits, defined as three times the standard deviation of the blanks, were 110, 51 and 81 nmol Si<sub>1</sub> respectively for ISP, ISP-SF and NSK. Blank measurements were also performed with new membranes processed directly in the clean lab (i.e. avoiding the blank due to water filtration on-board), which yielded detection limits of 1.5, 0.3 and 21 nmol Si<sub>1</sub> respectively for ISP, ISP-SF and NSK. The detection limit obtained by Ragueneau et al. (2005) ranges from 0.6 to 1.5 nmol Si<sub>1</sub>, which shows that Si contamination of our samples mostly comes from on-board manipulations. However, because blanks had unstable values and were not performed at each station, we decided not to subtract the blanks from our samples; yet we excluded samples with BSi concentrations lower than the detection limit. This concerns 22 NSK samples of 5 stations from the STZ (St. 2, 3, 8, 10 and 11). By doing so, the processing blank ( $Si_1 = 30.6$  nmol) is always lower than our lowest real sample ( $Si_1 = 87.3$  nmol). We acknowledge that BSi data slightly above our qualitative detection limit for NSK ( $Si_1 = 81$  nmol) have higher uncertainties.

Blank values for Al in the first leaching (Al $_1$ ) were 72.9  $\pm$  68.8 nmol for ISP and ISP-SF (n=9), and 294.1  $\pm$  171.3 nmol for NSK (n=9). Blank values for Al in the second leaching (Al $_2$ ) were 120.1  $\pm$  112.0 nmol for ISP and ISP-SF, and 70.2  $\pm$  49.9 nmol for NSK. The detection limits were 206 and 514 nmol Al $_1$  for respectively ISP plus ISP-SF and NSK, and 336 and 150 nmol Al $_2$  for respectively ISP plus ISP-SF and NSK. When Al $_1$  and Al $_2$  concentrations from a sample are lower than the detection limit, no lithogenic correction was applied. Hence, for these samples, BSi corresponds to Si $_1$ , and LSi to the sum of Si $_2$  and Si $_3$ . This method, called hereinafter "no correction", will be compared to the initial method from Ragueneau et al. (2005).

# 2.3. Hypotheses associated with BSi and LSi extractions

The protocol presented by Ragueneau et al. (2005) implies three main hypotheses. First, measured Al comes only from the lithogenic fraction, thus neglecting any BSi contribution; yet some Al is integrated in the silica matrix of the diatom frustules (Gehlen et al., 2002; Tian et al., 2022). Gehlen et al. (2002) report Al:Si ratios from Thalassiosira nordenskjiöldii frustules equal to  $1.3 \times 10^{-3}$  grown under Al concentrations of 9 nmol.L<sup>-1</sup> – which corresponds to the maximum concentrations observed in the Indian Ocean including its Southern sector (Thi Dieu, and H., and Y. Sohrin., 2013). Although this Al:Si ratio is very low, this Al interference can lead to an overestimation of LSi concentrations, in both offshore waters with low dissolved Al concentrations and in coastal areas with high dissolved Al (Van Bennekom et al., 1991; Ragueneau et al., 2005). However, we do not have any tool to measure diatom Al:Si ratios so we have to neglect the contribution of biogenic Al. Nevertheless, this potential error should be much smaller than the error from the correction and the reproducibility of the method since it concerns an overestimation of LSi from the first leaching, which represents on average 20% of  $\mathrm{Si}_1$  while the overall reproducibility of the method is 13% (see section 3.1 and 4.1). Second, the protocol imposes that BSi must be entirely digested in the first alkaline digestion (L1). According to Ragueneau et al. (2005) this implies that the BSi content of the sample should not exceed 10  $\mu mol$ , that no more BSi is dissolved during the second leaching, and that  $\mathrm{Si}_2:Al_2$  ratio of the second leaching should reflect the Si:Al ratio that is extracted from the lithogenic fraction. Third, the Si:Al ratios from LSi dissolved during the first and second alkaline digestion steps are assumed to be the same.

Another way to correct for the LSi contribution to BSi is by using a crustal lithogenic Si<sub>2</sub>:Al<sub>2</sub> ratio of 3.74 (Taylor and McLennan, 1985):

$$[BSi] = [Si]_1 - [Al]_1 *3.74.$$
 (3)

$$[LSi] = [Si]_3 + [Si]_2 + ([Si]_1 - [BSi]).$$
 (4)

where subscripts refer to # of leaching. This has been applied in the Kerguelen region by Fripiat et al. (2011a). This method, called hereinafter "average crustal ratio", will be compared to the initial method from Ragueneau et al. (2005).

#### 2.4. Scanning electron microscope (SEM) observations

Approximatively 50 mL of seawater sampled from Niskin bottles was immediately filtered on-board through polycarbonate membranes (Nuclepore®, 25 mm, 0.4 µm pore size) and processed with the same filtration units and conditions as for BSi NSK which includes rinsing the membrane with Milli-Q water to remove sea salt. Observations were carried out with a SEM (Zeiss EVO® LS15) operating at 15 kV at the Alysés analytical platform (Institut de Recherche pour le Développement – Sorbonne Université, IRD-SU, Bondy, France). Approximatively ¼ of each filter was beforehand glued to a metallic support and carbon coated. While biogenic particles were easily identifiable by their morphology, elemental spectra obtained with an energy dispersive X-ray microprobe (INCA Energy 350 system, Oxford Instruments®) coupled with the SEM were also used to identify lithogenic particles (mineral or at least mineralogical group).

15 samples from 12 stations selected from contrasting regions and from our BSi and LSi results were analysed using SEM-EDX. For each, a few pictures were taken at fixed magnifications in order to get an insight of the diversity and abundance of the biogenic and lithogenic materials. However, no particle counting was carried out, as our SEM research objectives were primarily (i) to check for the presence or absence of lithogenic materials, (ii) to identify these minerals when present and (iii) to check if silicifiers other than diatoms were present and could significantly contribute to the BSi pool.

#### 2.5. Pigment measurements

Between 1 and 2 L of seawater sampled from Niskin bottles was immediately filtered on-board through glass-microfiber membranes (Whatman® GF/F, 25 mm, 0.7  $\mu m$  pore size). Filters were then stored in 2.5 mL cryovials, flash-frozen in liquid nitrogen and stored at  $-80~^{\circ} C$  until analysis at the SAPIGH analytical platform (Institut de la Mer de Villefranche, IMEV, Villefranche-sur-Mer, France). Filters were analysed by HPLC pigment analysis described in Ras et al. (2008). Briefly, filters were extracted in 3 mL of 100% methanol, sonicated once and then clarified by filtration. Analysis of extracts was carried out within 24 h after extraction on a HPLC Agilent® Technologies 1200. In this study, we will use total chlorophyll a and fucoxanthin to support our BSi measurements.

#### 3. Results

All BSi and LSi data from either ISP, ISP-SF or NSK, and all total chlorophyll a and fucoxanthin pigments data are available in the Data

availability section.

# 3.1. Reproducibility of biogenic silica and lithogenic silicon

Although BSi is commonly measured to study the marine biogeochemical Si cycle, it is often not replicated, either with replicate samples or with replicate analysis or filter subsamples. We replicated 20 SWINGS samples (10 ISP + 10 NSK) by cutting each filter into three subsamples each filter, using the protocol. We selected the analytical replicated samples, called hereinafter "triplicates", from contrasting regions encompassing a wide range of BSi and LSi concentrations. Based on the relative standard deviation (RSD) results from the 20 triplicates, BSi and LSi show a mean and standard deviation respectively of  $25 \pm 17\%$  and  $47 \pm 37\%$  (Table 1). No significant differences were noticed between ISP and NSK RSDs, either for BSi (Kruskal-Wallis test: p-value = 0.11) or for LSi (Kruskal-Wallis test: p-value = 0.50). Although these values seem high, they are most of the time sufficient to discuss the differences between stations through the water column, as the concentrations are generally highly variable. Moreover, above the 1  $\mu$ mol L<sup>-1</sup> threshold and excluding an outlier (St. 44, ISP, 50 m; see explanation on Fig. 2), mean and standard deviations of the RSDs drop to a reproducibility of 13  $\pm$ 7% for both BSi and LSi (Fig. 2), which falls in the same range as Ragueneau et al. (2005) (11% for BSi and 7% for LSi, 1 standard deviation) as well as the RSDs reported by Krause et al. (2021) for BSi (9  $\pm$ 15% and 6  $\pm$  5% for upper and lower euphotic zone, respectively). The higher variability with the inclusion of the outlier probably comes from the ISP sample processing procedure: larger seawater volumes pumped, combined with the need of not exceeding 10 µmol for the first BSi digestion (see section 2.3), can result that a tiny portion (up to 3%) of the initial membrane was cut for the analysis. Thus, there is a risk that the BSi was not homogeneously distributed on the membrane.

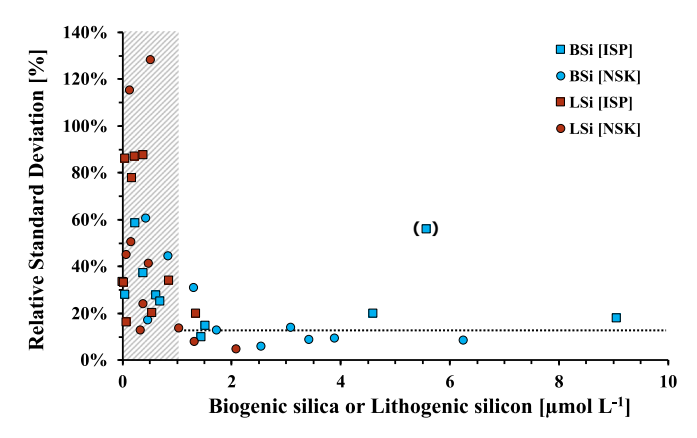


Fig. 2. Evolution of the relative standard deviation from replicates as a function of biogenic silica (BSi) or lithogenic silicon (LSi) concentrations, from Niskin bottles (NSK) and in situ pumps (ISP), using the correction method from Ragueneau et al. (2005). The grey hatched box covers the area where BSi or LSi concentrations are below 1  $\mu$ mol L $^{-1}$ . The black dashed horizontal line shows the reproducibility value of 13% from the relative standard deviations of triplicate samples, with BSi or LSi concentrations above 1  $\mu$ mol L $^{-1}$  (see section 3.1). The outlier excluded for the reproducibility calculation is represented in brackets. Results from a Dixon's test (0.752, with  $n=17,~x_n$  considered as potential outlier, r22=0.605<0.752, considering  $\alpha=0.005$ ) support the objective exclusion of this outlier from the small triplicate dataset (> 1  $\mu$ mol L $^{-1}$ ), despite shortcomings and limits of this test (Efstathiou, 2006).

By comparing both the initial Ragueneau et al. (2005) method (Eq. 1 & 2) and average crustal ratio method (Eq. 3 & 4), only two triplicates have significant differences for BSi between the two methods (Kruskal-Wallis test: p-value <0.05). Both triplicates in question are ISP samples

Table 1
Replicates performed on 10 Niskin bottle samples (NSK) and 10 *in situ* pumps samples (ISP). Values of biogenic silica (BSi), lithogenic silicon (LSi) and their relative standard deviation (RSD) correspond to mean  $\pm$  standard deviation. Means that are not significantly different (Kruskal-Wallis test: p-value >0.05) are labelled with the same letter within a replicate. Acronyms for BSi and LSi values correspond to the three correction methods: RAG = correction from the initial Ragueneau et al. (2005) method (Eq. 1 & 2); ACR = Average Crustal Ratio method (Eq. 3 & 4); NOC = No correction. KERFIX and A3 annotations refer to two reference stations sampled on previous oceanographic cruises around the Kerguelen Plateau, respectively KERFIX and KEOPS programs (Jeandel et al., 1998; Blain et al., 2008).

Station	Features	Type	Depth	Bioge	nic silica (BSi) [μmo	l L <sup>-1</sup> ]	Lithogenic silicon (LSi) [ $\mu$ mol L <sup>-1</sup> ]			
		<u> </u>	[m]	RAG	ACR	NOC	RAG	ACR	NOC	
11	STZ	ISP	70	$0.05 \pm 0.01^{a}$	$0.05 \pm 0.02^{a}$	$0.05 \pm 0.02^{a}$	$0.01 \pm 0.00^{a}$	$0.01 \pm 0.00^{a}$	< 0.01 <sup>a</sup>	
25	PFZ	ISP	30	$0.62\pm0.17^a$	$0.66\pm0.18^a$	$0.67\pm0.18^a$	$0.08\pm0.01^a$	$0.03\pm0.01^{\mathrm{b}}$	$0.03\pm0.01^{\rm b}$	
		ISP	60	$0.24\pm0.14^a$	$0.37\pm0.03^{\mathrm{b}}$	$0.37\pm0.03^{\mathrm{b}}$	$0.17\pm0.13^a$	$0.04\pm0.01^{b}$	$0.04\pm0.01^{b}$	
		ISP	250	$0.70\pm0.18^a$	$0.71\pm0.17^a$	$0.71\pm0.17^a$	$0.02\pm0.01^a$	$0.01\pm0.00^a$	$0.01\pm0.00^{\mathrm{b}}$	
		ISP	3655	$0.38\pm0.14^a$	$0.71 \pm 0.05^{b}$	$0.82\pm0.10^{\rm b}$	$0.54\pm0.11^a$	$0.22\pm0.05^{\mathrm{b}}$	$0.10\pm0.02^{c}$	
42	KERFIX	ISP	25	$1.52\pm0.23^a$	$1.68\pm0.13^a$	$1.68\pm0.13^a$	$0.23\pm0.20^a$	$0.07 \pm 0.04^{a}$	$0.07\pm0.04^a$	
44	Heard Island	ISP	50	$5.57 \pm 3.11^{a}$	$5.64 \pm 3.02^{a}$	$6.69 \pm 3.31^{a}$	$1.35\pm0.27^a$	$1.28\pm0.57^a$	$0.23\pm0.04^{\rm b}$	
		NSK	60	$1.74\pm0.22^a$	$1.64\pm0.19^a$	$2.01\pm0.20^a$	$0.34\pm0.04^a$	$0.44\pm0.13^a$	$0.06\pm0.02^{\rm b}$	
46	Heard Island	NSK	30	$2.55\pm0.15^a$	$1.89\pm0.62^a$	$3.36\pm0.27^{\rm b}$	$1.04\pm0.14^a$	$1.70\pm0.46^{\mathrm{b}}$	$0.23\pm0.03^{c}$	
		NSK	100	$6.26\pm0.54^a$	$5.36\pm0.91^a$	$7.83\pm0.58^{\mathrm{b}}$	$2.09\pm0.10^a$	$2.99\pm0.91^a$	$0.52\pm0.07^{\mathrm{b}}$	
58	AZ	ISP	30	$9.06\pm1.63^a$	$9.25\pm1.63^a$	$9.27\pm1.65^a$	$0.38\pm0.33^a$	$0.20\pm0.19^a$	$0.17\pm0.16^a$	
		NSK	40	$3.10\pm0.43^a$	$3.47\pm0.37^a$	$3.49\pm0.38^a$	$0.52\pm0.67^a$	$0.14\pm0.15^a$	$0.13\pm0.14^{a}$	
63	"Fawn Trough"	NSK	40	$0.84\pm0.37^a$	$0.93\pm0.48^a$	$0.94 \pm 0.48^{a}$	$0.14\pm0.16^a$	$0.05 \pm 0.06^{a}$	$0.04\pm0.05^a$	
		NSK	60	$0.47\pm0.08^a$	$0.57\pm0.10^a$	$0.59\pm0.10^a$	$0.16\pm0.08^a$	$0.06 \pm 0.06^{a}$	$0.04\pm0.05^a$	
65	MacDonald island	NSK	120	$3.89\pm0.36^a$	$3.28\pm0.28^a$	$4.96\pm0.39^{\mathrm{b}}$	$1.33\pm0.11^a$	$1.94 \pm 0.67^{a}$	$0.26\pm0.02^{\rm b}$	
68	A3	ISP	30	$1.45\pm0.15^a$	$1.48\pm0.17^a$	$1.49\pm0.17^a$	$0.05\pm0.04^a$	$0.02\pm0.01^a$	$0.01\pm0.01^a$	
		NSK	40	$1.31\pm0.41^a$	$1.34\pm0.42^a$	$1.36\pm0.43^a$	$0.08\pm0.04^a$	$0.05\pm0.03^a$	$0.04\pm0.02^a$	
		NSK	80	$0.43\pm0.26^a$	$0.75\pm0.08^a$	$0.79\pm0.05^a$	$0.49\pm0.20^a$	$0.17\pm0.05^{\mathrm{b}}$	$0.13\pm0.08^{\rm b}$	
		ISP	430	$4.60\pm0.91^a$	$5.06\pm0.80^a$	$5.35\pm0.89^a$	$0.86\pm0.29^a$	$0.40\pm0.18^a$	$0.11\pm0.05^{\mathrm{b}}$	
		NSK	459	$3.43\pm0.30^a$	$3.51\pm0.27^a$	$3.75\pm0.27^a$	$0.39\pm0.09^a$	$0.31\pm0.10^{a}$	$0.07\pm0.01^{\mathrm{b}}$	

Station	Features	Type	Depth	Biogenic silica (BSi) RSD [%]			Lithogenic silicon (LSi) RSD [%]		
			[m]	RAG	ACR	NOC	RAG	ACR	NOC
All replicates	All replicates (ISP)		_	$30\pm16$	$20\pm14$	$20\pm13$	$50\pm31$	$45\pm22$	$46\pm23$
All replicates	(NSK)	NSK	_	$21\pm18$	$20\pm14$	$16\pm15$	$44\pm44$	$55\pm35$	$54 \pm 46$
All replicates (ISP + NSK) -		-	-	$25\pm17$	$20\pm14$	$18\pm14$	$47\pm37$	$50\pm28$	$50\pm35$

STZ = Subtropical Zone; PFZ = Polar Frontal Zone; AZ = Antarctic Zone.

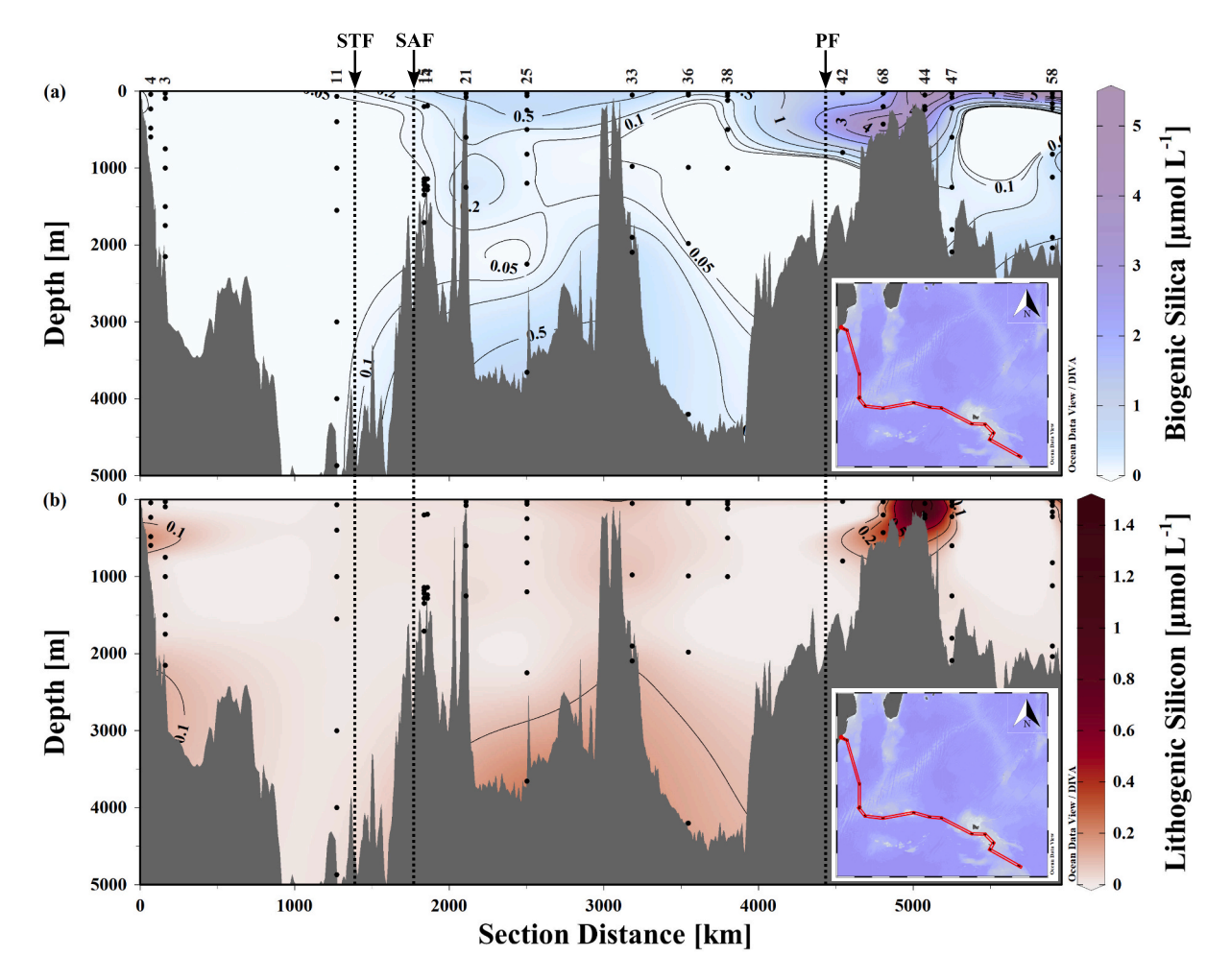
with relatively low BSi concentrations ( $< 0.4 \mu mol L^{-1}$ , see Table 1). For LSi, five triplicates have significant differences between the two methods (Kruskal-Wallis test: p-value <0.05). Both initial Ragueneau et al. (2005) and average crustal ratio methods are thus generally coherent, especially for BSi NSK samples that represent most of our BSi data. Therefore by default, the initial method from Ragueneau et al. (2005) will preferentially be used for lithogenic correction, as it considers the Si<sub>2</sub>:Al<sub>2</sub> ratio fluctuations among samples rather than a global crustal ratio. This implies also that both Al<sub>1</sub> and Al<sub>2</sub> are above detection limit. If Al<sub>1</sub> is below detection limit, then no correction is applied. This concerns 128 NSK samples, 14 ISP samples and 87 ISP-SF samples. Finally, when the 10  $\mu$ mol threshold of Si<sub>1</sub> is exceeded and/or Al<sub>2</sub> concentrations are lower than the detection limit (see section 2.2), BSi and LSi concentrations will be calculated with the average crustal ratio method. This concerns 7 out of 189 NSK samples, 34 out of 78 ISP samples and 56 out of 170 ISP-SF samples.

#### 3.2. Distribution of biogenic silica, total chlorophyll a and fucoxanthin

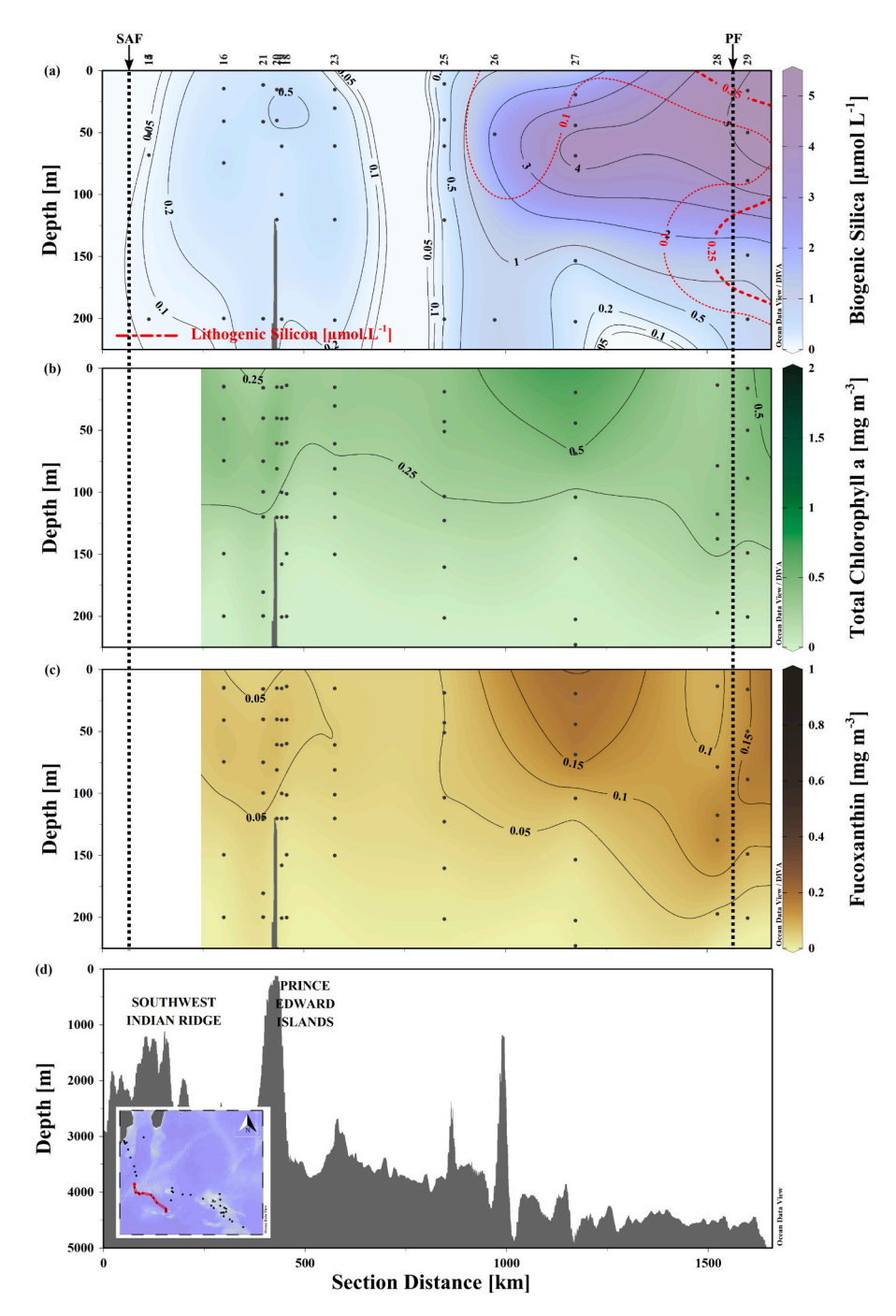
Results are displayed in several oceanic sections: one global section displaying all ISP samples values (Fig. 3) and three sub-sections, starting south of the SAF and displaying NSK samples values (Fig. 4, 5 and 6). Most NSK BSi concentrations north of the SAF (St. 2, 3, 8, 10 and 11) are under the detection limit (see section 2.2). Only St. 4 close to the South African margin was above the detection limit and showed BSi concentrations  $<\!0.07~\mu\mathrm{mol}~L^{-1}$  (Fig. 3, Fig. S1).

Fig. 3 highlights the BSi gradient between the biogeochemical provinces encountered. BSi concentrations in the STZ were the lowest measured throughout this section and did not exceed 0.05  $\mu$ mol L<sup>-1</sup>. To the south, BSi content in the PFZ increased gradually, ranging up to 0.7 μmol L<sup>-1</sup> in the first hundred meters and decreased in the deep waters to  $<0.1 \mu mol L^{-1}$ . South of the PF in the AZ, high and variable BSi concentrations were measured. First, in the surface waters, HNLC stations (St. 42 and 47) had lower BSi concentrations  $(1.7-3.7 \mu mol L^{-1})$  than naturally fertilized stations (St. 44:  $3.9-5.6 \mu mol L^{-1}$ ). Nevertheless, BSi at St. 58 in an HNLC region reached 9.1  $\mu$ mol L $^{-1}$  and St. 68 (A3) in a naturally fertilized regime was in the same range as HNLC stations. Second, higher BSi concentrations were observed at the bottom of the Kerguelen Plateau compared to those in the deep waters, independent of the sampling method (St. 44, 68: ISP:  $3.9-5.1 \mu mol L^{-1}$ ; NSK: 1.9-3.4 $\mu$ mol L<sup>-1</sup>; Fig. 3, Fig. S1). This increase in bottom waters also occurred but to a lesser extent at several HNLC stations in the PFZ (St. 25, 33, 36;  $0.3-0.7 \mu mol L^{-1}$  Fig. 3). These increases of BSi in bottom waters were not associated to any chlorophyll a increase as measured with the fluorescence sensor on the CTD-Rosette (data not shown).

Focusing on NSK samples in the first 200 m (Fig. 4, 5 and 6), BSi concentrations are highly variable depending on the biogeochemical provinces. The "NW-SE" section (Fig. 4) emphasizes a BSi gradient from the PFZ (0.1–1.3  $\mu$ mol L $^{-1}$ ) to the AZ, reaching at the surface 5.3  $\mu$ mol L $^{-1}$  at St. 29. Even though they are in the PFZ, St. 26 and 27 also had higher BSi and LSi than other PFZ stations. The "W-E" (Fig. 5) and "Kerguelen Plateau" (Fig. 6) subsections show stations around the



**Fig. 3.** Vertical distribution in the whole water column of (a) BSi (black isolines and interpolation) and (b) LSi (black isolines and interpolation), both from *in situ* pumps, with GEBCO bathymetry along the section "04-58 – Global section". The dotted lines represent the approximate positions of the Southern Ocean fronts crossed during the SWINGS cruise. STF = subtropical front; SAF = subantarctic front; PF = polar front. Sections from Ocean Data View (Schlitzer, 2024).



**Fig. 4.** Vertical distribution in the first 200 m of (a) BSi (black isolines and interpolation) and LSi (red dotted isolines) from Niskin bottles, (b) total chlorophyll a and (c) fucoxanthin with (d) GEBCO bathymetry along the section "14-29 – NW-SE". The dotted lines represent the approximate positions of the Southern Ocean fronts crossed during the SWINGS cruise. SAF = subantarctic front; PF = polar front. Sections from Ocean Data View (Schlitzer, 2024).

different Subantarctic islands which have contrasting BSi concentrations. On the one hand, stations near the Prince Edward Islands and Crozet archipelago follow the same pattern, with BSi ranging from 0.3 to 0.6  $\mu mol~L^{-1}$  (Fig. 5). One exception is St. 35 near the East island of Crozet, with a BSi maximum of 2.5  $\mu mol~L^{-1}$ , which drops to the previous low range in the subsurface. On the other hand, stations around the Kerguelen Plateau show much higher BSi concentrations, ranging from 1.1 to 3.9  $\mu mol~L^{-1}$ , with a peak of 5.4  $\mu mol~L^{-1}$  at the bottom of St. 46 (Fig. 6). As for ISP samples, BSi at St. 58 in HNLC regime was higher than other HNLC stations in the AZ, reaching 3.7  $\mu mol~L^{-1}$  at the surface. For the three NSK transects (Fig. 4, 5 and 6), the vertical distribution

of BSi generally mirrors that of fucoxanthin. This is particularly the case on Fig. 4 and the southern parts of the transect (Fig. 5 and 6) while St. 66 displays a strong fucoxanthin maximum with limited BSi. The vertical distribution of chlorophyll a follows a pattern like fucoxanthin except in Fig. 5. Maxima of fucoxanthin (1.1 mg.m $^{-3}$ ) and chlorophyll a (3.1 mg. m $^{-3}$ ) were observed at St. 66 where a phytoplankton bloom occurred off Heard Island (Fig. 6). BSi concentrations observed during this bloom, ranging from 1.5 to 3.3  $\mu$ mol L $^{-1}$ , were not as high as other stations that showed much lower pigment concentrations, such as St. 29 (5.3  $\mu$ mol L $^{-1}$ ) or St. 58 (3.7  $\mu$ mol L $^{-1}$ ).

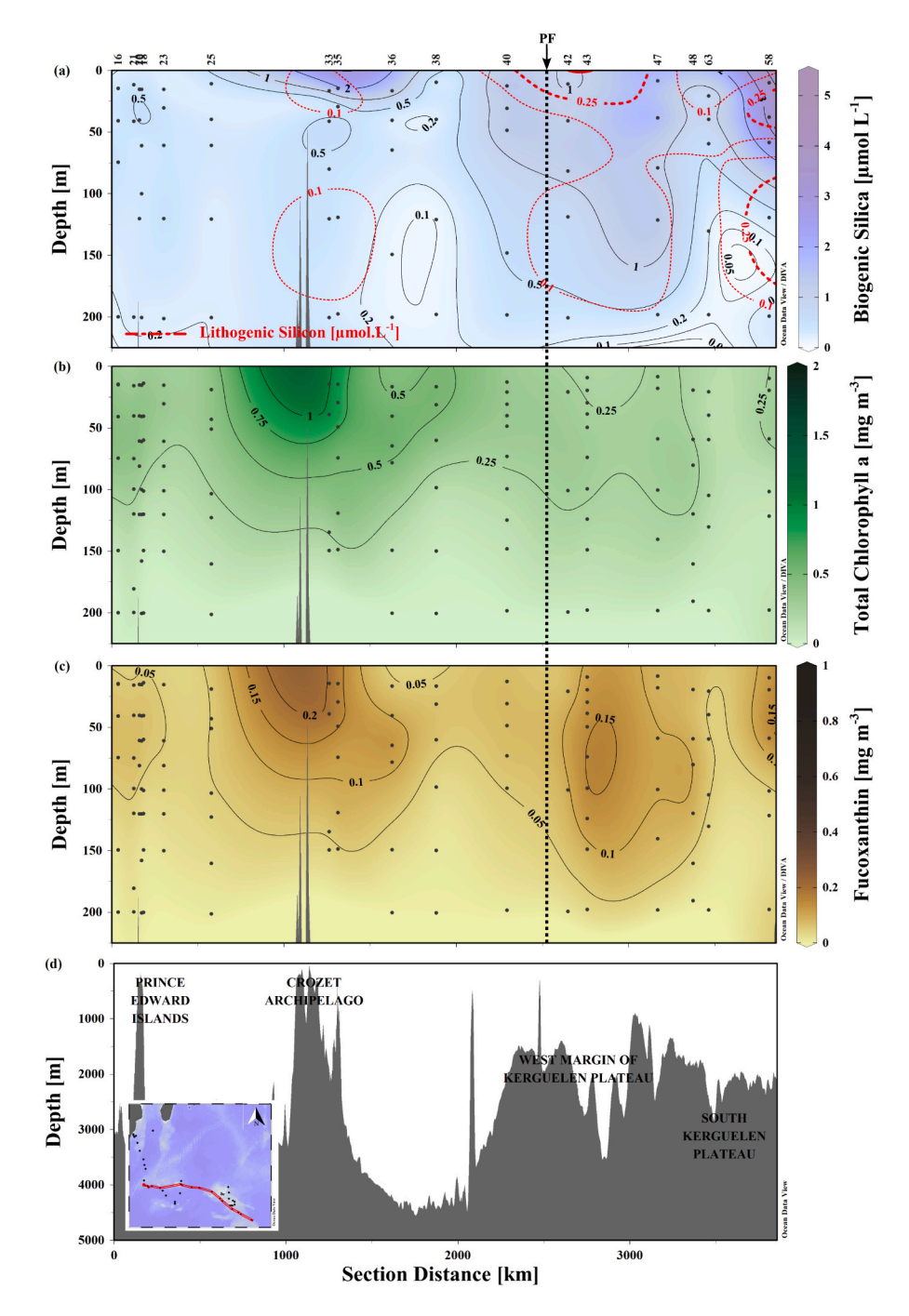


**Fig. 5.** Vertical distribution in the first 200 m of (a) BSi (black isolines and interpolation) and LSi (red dotted isolines) from Niskin bottles, (b) total chlorophyll *a* and (c) fucoxanthin with (d) GEBCO bathymetry along the section "16-58 – W-E". The dotted lines represent the approximate positions of the Southern Ocean fronts crossed during the SWINGS cruise. PF = polar front. Sections from Ocean Data View (Schlitzer, 2024).

# 3.3. Distribution of size-fractioned biogenic silica

Size fractionation of BSi can complement the description of the diatom communities by providing information on their sizes, even though the presence of biogenic fragments can alter this information. Fraction of 5–53  $\mu m$ , comprised of most of the nano-sized (3–20  $\mu m$ ) and some micro-sized (> 20  $\mu m$ ) BSi, can correspond to small and medium diatom species. Fraction >53  $\mu m$ , comprised of the large micro-sized BSi, can correspond to large diatom species, large colonies of diatoms and sometimes Rhizaria. The fraction 0.4–5  $\mu m$ , which can correspond to small and fragmented diatoms and Si in Synechococcus sp. (Baines et al., 2012), can be derived from the difference between the ISP > 0.45

 $\mu m$  and the sum of ISP-SF data. Note that Synechococcus sp. is likely to contribute in the subtropical zone but not in the Southern Ocean regarding zeaxanthin concentrations and Fuco:Zeaxanthin ratios (data not shown). However, the sampling depth sometimes differs slightly between ISP and ISP-SF (Fig. S1).

# 3.4. Distribution of lithogenic silicon

In the open ocean stations, LSi concentrations remained very low and did not exceed  $0.1~\mu\text{mol}~L^{-1}$  throughout most of the water column. However, some exceptions were noted, in the surface at St. 26 to 29 and 58, where LSi concentrations were slightly higher, sometimes reaching

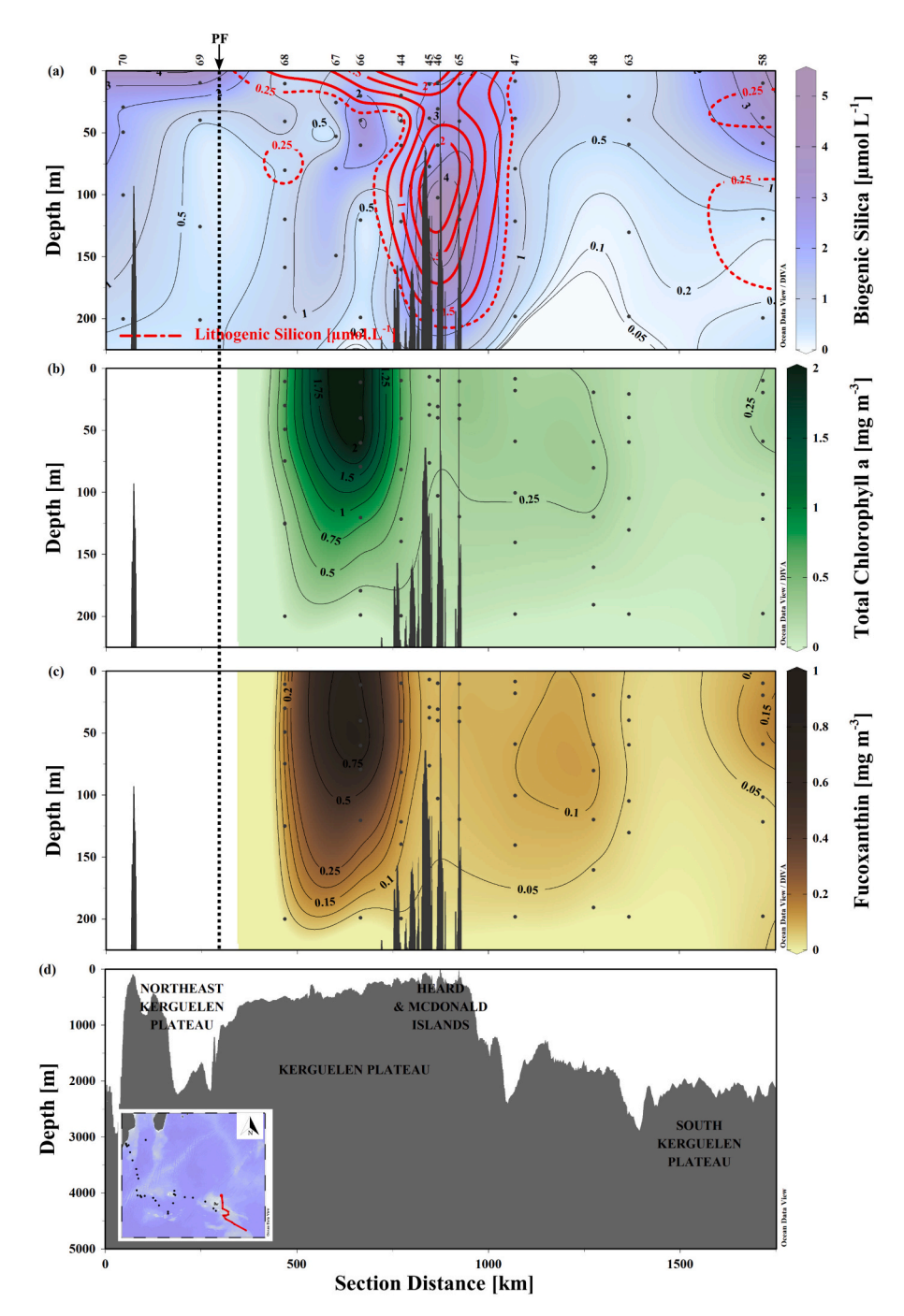


**Fig. 6.** Vertical distribution in the first 200 m of (a) BSi (black isolines and interpolation) and LSi (red dotted isolines) from Niskin bottles, (b) total chlorophyll *a* and (c) fucoxanthin with (d) GEBCO bathymetry along the section "58-70 – Kerguelen Plateau". The dotted lines represent the approximate positions of the Southern Ocean fronts crossed during the SWINGS cruise. PF = polar front. Sections from Ocean Data View (Schlitzer, 2024).

0.3 µmol L $^{-1}$  (Fig. 4). Similarly, stations in the vicinity of the Subantarctic islands displayed higher LSi concentrations compared to open ocean stations. Maxima were observed around Heard Island: at St. 45 and 46 LSi values were >2.0 µmol L $^{-1}$ , with a peak of 3.0 µmol L $^{-1}$  at 100 m depth for St. 46. Stations near the Crozet archipelago and in the Southern African margin were characterised by much lower LSi concentrations, reaching a maximum of 0.2 µmol L $^{-1}$  (Fig. 3 and 5). On the other hand, LSi values from stations near the Prince Edward Islands were like open ocean stations. As for BSi, higher LSi concentrations were also observed at the bottom of several stations compared to those in deep waters. This concerns St. 68 above the Kerguelen Plateau (0.4 µmol L $^{-1}$ ) and several open ocean stations in the PFZ quoted above (see section

3.2): e.g. St. 25 and 36 (0.1–0.2  $\mu$ mol L<sup>-1</sup> Fig. 3). Similar increases were observed in the subsurface of St. 42 (0.3  $\mu$ mol L<sup>-1</sup> at 120 m) and St. 68 (0.5  $\mu$ mol L<sup>-1</sup> at 80 m) by the Kerguelen Plateau.

# 3.5. Scanning electron microscope observations

Observations performed by SEM revealed the presence of both biogenic and lithogenic material in suspended particles collected along the SWINGS transect. Focusing first on the biogenic fraction within surface samples, a biogenic abundance typical of the previous north-south gradient was observed (Fig. S2): starting with a very low abundance of diatoms and coccolithophores in the STZ (Fig. S2a) contrasted

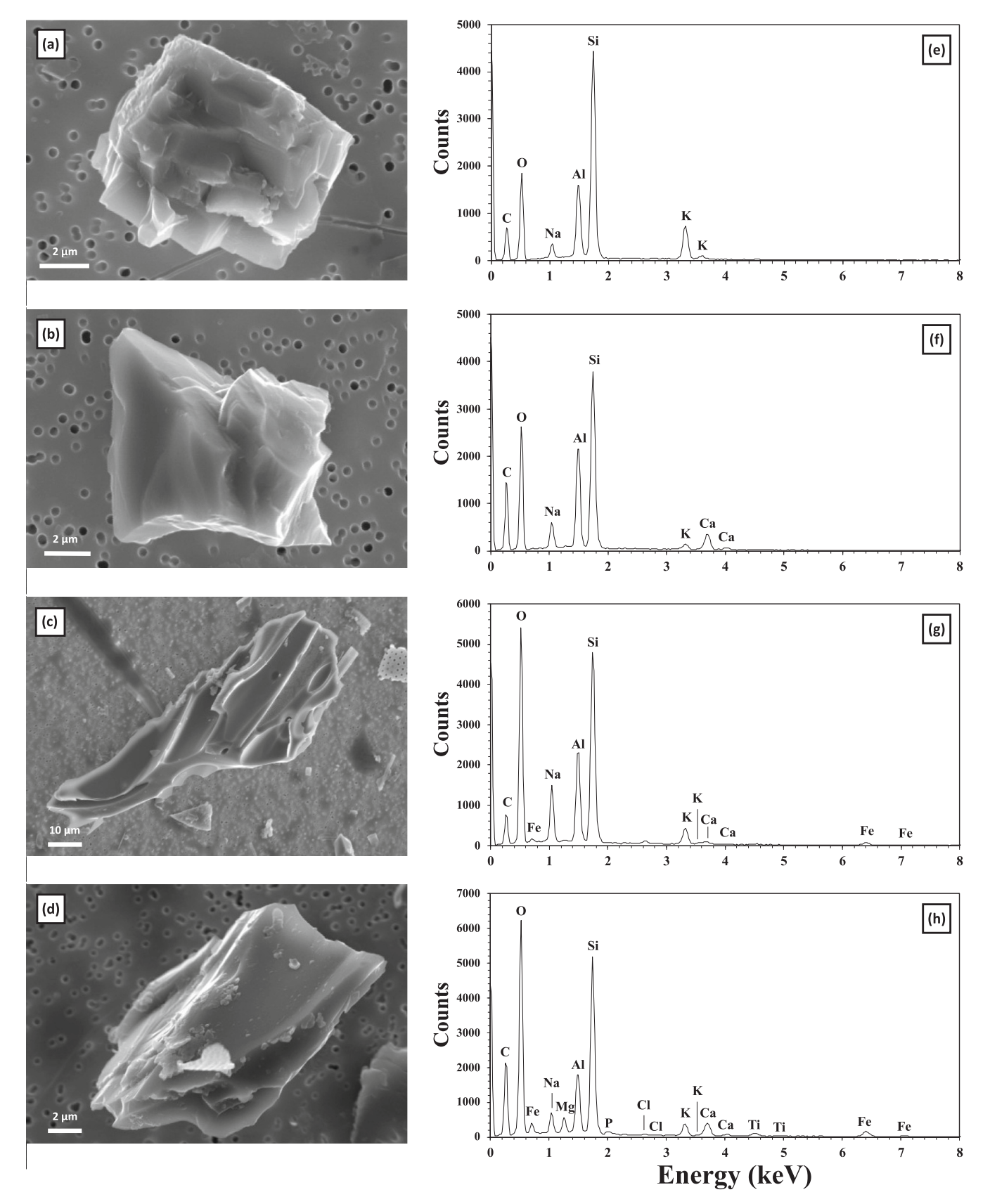


Fig. 7. SEM pictures of lithogenic particles collected at the surface near Heard (St. 46) and MacDonald Islands (St. 65), with their respective EDX spectrum. (a) and (e) Alkali feldspar at St. 65; (b) and (f) Plagioclase feldspar at St. 65; (c) and (g) Volcanic ash at St. 65; (d) and (h) Volcanic ash at St. 46.

with a predominance of diatoms in the AZ (Fig. S2g) or around the Subantarctic islands (Fig. S2j). Among siliceous phytoplankton, some silicoflagellates and chrysophytes (Fig. S2i and S2l, respectively) were noticed in the Kerguelen Plateau stations and few Rhizaria from ISP samples were observed (data not shown), but they represented only a minor fraction in all samples in comparison to diatoms (Fig. S2i and S2l). Diatoms from the Kerguelen Plateau stations were more fragmented than those at the HNLC stations, whereas St. 58 displayed the least degraded and the most diverse diatom community, including small, medium and large diatoms. These SEM observations are consistent with our previous results for size fractioned BSi and support them by clearly indicating that the 0.45–5  $\mu m$  fraction is mainly composed of diatom fragments at St. 44 (see section 3.3).

In addition, SEM observations identified lithogenic material (i) primary minerals such as feldspars (Fig. 7a and b) and amphiboles (not shown) mainly in the Kerguelen Plateau and (ii) volcanic ashes (Fig. 7c and d) near Heard and MacDonald Islands. EDX data (Fig. 7e to 7h) indicates a predominance of alkali feldspars ((K,Na)[AlSi<sub>3</sub>O<sub>8</sub>]) compared to plagioclase feldspars (Na<sub>x</sub>Ca<sub>1-x</sub>Al<sub>2-x</sub>Si<sub>2+x</sub>O<sub>8</sub>). Volcanic ash particles can be distinguished by both their morphologies (angular, vesicular pumiceous particles) and/or their more complex chemical composition (Si, Al, Na, K, along with traces of Mg, Cl, Fe, and sometimes P and Ti). Some primary minerals and volcanic ashes were also observed in two bottom samples at St. 36 in the PFZ and St. 68 (A3), which is consistent with the LSi results (see section 3.4).

#### 4. Discussion

#### 4.1. Relevance and limits of the methods via aluminium correction

The method proposed by Ragueneau et al. (2005) clearly states it applies especially for coastal waters to more adequately correct high lithogenic interferences during the first leaching. This protocol was already applied for samples collected in both open ocean regions and continental-influenced areas in previous cruises (Mosseri et al., 2008; Fripiat et al., 2012). Nevertheless, it remains delicate in open ocean areas, where LSi concentrations are very low and with high BSi. When BSi particles count for an important fraction of the collected suspended matter, Al interference in diatom frustules can lead to a BSi underestimation (Ragueneau et al., 2005). For instance, Lasbleiz et al. (2014) proposed not to apply an aluminium correction for open ocean samples as Al can be dominated by biogenic phases. In our samples where the Ragueneau et al. (2005) correction was applied (i.e. mainly continentalinfluenced samples), the correction remains small since BSi represents 79% of the fraction from the first leaching (NSK: 77%; ISP: 77%; ISP-SF: 84%).

For some samples satisfying all criteria from the Ragueneau et al. (2005) method, measured Si<sub>2</sub>:Al<sub>2</sub> ratio can be still variable and even high, suggesting that the lithogenic fraction from the second leaching was Al-depleted. As an example, some samples showed high LSi concentrations (St. 29: 0.29  $\mu$ mol L<sup>-1</sup>; St. 68: 0.13  $\mu$ mol L<sup>-1</sup> at 80 m, Fig. 6) and also displayed high Si<sub>2</sub>:Al<sub>2</sub> ratios (respectively 126 and 95). Unfortunately, no SEM samples were collected at the latter depths. However, some Al-free primary minerals, such as quartz (SiO2) or olivine ((Mg,Fe)2[SiO4]) were observed in St. 68 at 120 m, although its LSi and  $Si_2$ :Al $_2$  values were lower (LSi = 0.01  $\mu$ mol L $^{-1}$ ;  $Si_2$ :Al $_2$  = 9). Assuming by interpolation that high LSi concentrations at St. 29 and 68 are related to Al-free minerals, their presence emphasizes the importance of the sequential digestions in the Ragueneau et al. (2005) method and thus the importance of using individual Si<sub>2</sub>:Al<sub>2</sub> ratio. Otherwise, using an average crustal Si:Al ratio would underestimate LSi by excluding potential Al-free minerals, and consequently overestimate BSi.

An alternative would be to apply a correction of lithogenic interference with titanium (Ti) to limit the issue of Al assimilation in diatom frustules. This correction has already been applied on biogenic materials, either siliceous or even calcareous (Murray et al., 1993; Blain et al.,

2022). However, Cardinal et al. (2001) have reported that samples from the Australian sector of the Southern Ocean contain a great fraction of authigenic Ti, *i.e.* precipitated in the water column. Moreover, Ticontaining particles and aggregates, from 1 to  $\sim$ 100  $\mu$ m have been observed in most of our samples during SEM observations, ruling out the use of Ti for correcting lithogenic interferences.

Nevertheless, an important outcome of the reproducibility we have tested between the Ragueneau et al. (2005) and average crustal ratio methods is that they provide BSi results not significantly different for 18 out of 20 samples, and their reproducibility is comparable (Table 1). This indicates that even when different methods have been used in previous works in the Southern Ocean (e.g. Fripiat et al. (2011a) vs Lasbleiz et al. (2014) vs this study), data can still be compared.

#### 4.2. Lithogenic silicon as a tracer of lithogenic matter sources

#### 4.2.1. Synoptic view

In the study area, LSi concentrations generally do not exceed 0.10  $\mu mol~L^{-1}$  or 10 mmol  $m^{-2}$  when integrated over 200 m depth (Fig. 8b). These concentrations are in the same range as those measured previously in the South Indian and Southern Oceans:  $<0.03~\mu mol~L^{-1}$  in the STZ of Australian sector (Quéguiner, 2001),  $<0.14~\mu mol~L^{-1}$  in the SAZ of the South Indian sector (Leblanc et al., 2002) and  $<0.10~\mu mol~L^{-1}$  in the PFZ of either the South Atlantic or the Australian sector (Quéguiner et al., 1997; Quéguiner, 2001). Near but outside the Kerguelen Plateau, Lasbleiz et al. (2014) report several stations equivalent to St. 42 and 69, with LSi concentrations  $<0.10~\mu mol~L^{-1}$  typical of the open ocean.

However, we identified a few continentally-influenced stations with higher LSi contents (> 10 mmol.m<sup>-2</sup> when integrated over 200 m; Fig. 8b). For instance, high LSi concentrations, observed at the surface of St. 26, 27 and 29 south of the PF, were most likely caused by atmospheric inputs (Fig. 4 and 8b). Indeed, the first results of aerosol deposition measurements performed during the cruise show that these stations were characterised by the highest aerosol deposition over the entire SWINGS section. Moreover, 10-day back-trajectories generated with the NOAA HYSPLIT (Hybrid Single-Particle Lagrangian Integrated Trajectory) model suggest a desert origin for these atmospheric inputs, more specifically from Patagonia. Dust from this region has been shown to be able to reach the Southern Ocean (Li et al., 2008). In section 4.3.3 we discuss the potential impact of this lithogenic aeolian supply on diatoms.

# 4.2.2. Heard and MacDonald Islands

Mosseri et al. (2008) reported LSi values not exceeding 0.7  $\mu$ mol L<sup>-1</sup> during the KEOPS cruise, in the Kerguelen Plateau region. This is very consistent with our results with LSi  $< 0.73 \mu mol L^{-1}$ . There is an exception for one station close to Heard Island, where the lithogenic Si fraction reached  $32 \pm 8\%$  of total particulate Si in Mosseri et al. (2008). In our study, stations near Heard Island (St. 45 and St. 46) and Mac-Donald island (St. 65) have also a LSi fraction of 42  $\pm$  11% (LSi = 1.95  $\pm$  0.65  $\mu$ mol L<sup>-1</sup>) for Heard Island and of 30  $\pm$  5% (LSi = 1.25  $\pm$  0.08 μmol L<sup>-1</sup>) for MacDonald Island and integrated LSi exceed 200 mmol. m<sup>-2</sup> (Fig. 8b). SEM observations showed that basaltic primary minerals such as feldspar, accompanied by volcanic ashes, dominated these lithogenic fractions (Fig. 7). Previous works have shown that these volcanic ashes come from a phreatomagmatic hotspot volcanism and have a basaltic with phonolite tendency composition (Wise Jr. et al., 1992; Quilty and Wheller, 2000; Fox et al., 2021). Despite the low nutrient solubility from volcanic ashes reported by Geisen et al. (2022), their study showed that the nutrient concentrations released by ashes were equal for Si and higher for Fe compared to those released by Patagonian dust. Ash deposition could play a role in supplying bioavailable Fe and Si in the vicinity of Heard and McDonald Islands which are active volcanoes (in contrast to Kerguelen) –, especially in late austral summer when Si(OH)4 is depleted after being consumed by diatoms during the spring blooms over the Kerguelen Plateau (Closset

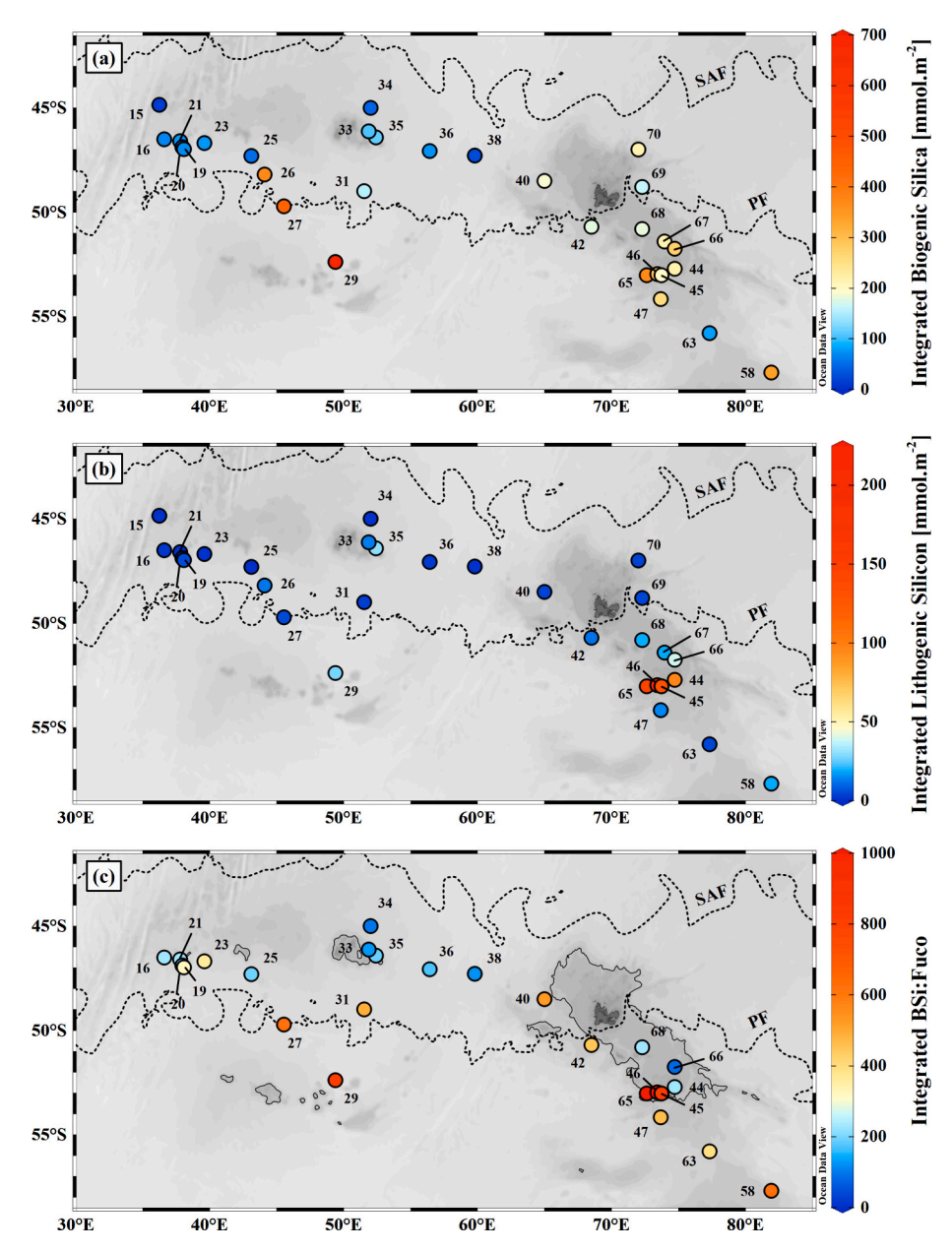


Fig. 8. (a) Integrated BSi, (b) integrated LSi and (c) integrated BSi:Fuco ratios from NSK data for stations in the Polar Frontal Zone and in the Antarctic Zone. Data have been integrated between 0 and 200 m depth. The labels correspond to the SWINGS station number. The black lines represent 1000 m isobath from GEBCO bathymetry. The dotted lines represent the positions of the Southern Ocean fronts determined from satellite-derived surface temperature averaged over February 2021 (CMEMS L4 product): SAF = Subantarctic Front (13 °C); PF = Polar Front (4.5 °C). Figure from Ocean Data View (Schlitzer, 2024).

et al., 2014). Such lithogenic supply of nutrients around Heard Island during KEOPS was already hypothesized from Si and Ra isotopes (van Beek et al., 2008; Fripiat et al., 2011). Recent studies also highlight the importance and magnitude of glacial erosion phenomenon from Heard Island in supplying bioavailable Fe and Si (van der Merwe et al., 2019).

### 4.2.3. Nepheloid layers

We observed several LSi increases (Fig. 3) often associated with an increase of turbidity corresponding to nepheloid layers, *i.e.* resuspended particles (McCave, 2009), at the bottom (St. 25, 33 and 36 in the PFZ) or at the margin of continental slopes (St. 4). Such increase was also observed at the bottom of St. 68 on the Kerguelen Plateau (~ 500 m) associated with high BSi concentrations, as already reported in previous studies (Lasbleiz et al., 2014; Closset et al., 2016). The nepheloid layers are likely reflecting a resuspension of BSi-rich and clay mineral-rich

(mainly illite and smectite) sediments (Borchers et al., 2011) which can release significant quantities of micronutrients (Fe and Mn), and which fertilize water masses over the Kerguelen Plateau (Blain et al., 2007; Cheize et al., 2019).

However, LSi increases observed at the subsurface of St. 42 and 68 are more difficult to explain, since these stations are far from continental influence (Fig. 6 and 8). This was also observed during KEOPS at A3 station, equivalent to St. 68. These features are perhaps due to an intermediate nepheloid layer coming from different seamounts around the Kerguelen Plateau, possibly transported by the ACC (Park et al., 2008). The potential seamounts, both peaking at 50 m below the surface, would be the Leclaire Rise Seamount (65°E, 50°S) for St. 42, and Pike Bank (70.5°E, 51.3°S) for St. 68.

#### 4.3. Biogenic silica as an indicator of diatoms in the Southern Ocean

#### 4.3.1. Synoptic view

The Southern Ocean surface waters become Si(OH)<sub>4</sub> depleted more rapidly northwards due to the Si(OH)4 trapping in the deep waters compared to N and P, which are remineralized at a shallower depth and can be more efficiently brought back to the surface by mixing (Sarmiento et al., 2004; Nissen et al., 2021). Stations located south of the PF have high surface Si(OH)<sub>4</sub> concentrations (> 10 μmol L<sup>-1</sup>, Fig. S3), precluding Si limitation for siliceous primary production, which is consistent with the highest BSi values at St. 29 (Fig. 4) and those in the Kerguelen Plateau (Fig. 3 and 6). From size-fractioned BSi results within the first 200 m (Fig. S1, n = 29), we estimate that the fraction 0.45–5  $\mu$ m accounts for 47  $\pm$  23% of the BSi in the region with no significant differences between the STZ, PFZ and AZ. The particles contributing to the small-size fraction can be identified from SEM observations. For instance, St. 44 has the highest proportion of this BSi fraction  $0.45–5~\mu m$ (77%), with lots of BSi fragments from diatoms (Fig. S2j and S2k). But there are also some small siliceous phytoplankton skeletons, either entire diatoms (St. 58, Fig. S2i) or Chrysophyceae (Fig. S2l). Therefore, even though our SEM observations are not quantitative, they shed light on the different particle types contributing to the small size BSi fraction. Nevertheless, SEM observations confirmed that diatoms dominate the siliceous phytoplankton (either as fragment or well-preserved frustules) and illustrate differences in diatom abundance between stations (Fig. S2). The decreasing BSi gradient from the AZ to the STZ can be attributed to a decrease in diatom abundance and a shift from a microphytoplankton community towards nano- and picophytoplankton (Geisen et al., 2022).

Comparison of BSi results in our study with previous oceanographic cruises is reported, for integrated BSi results between 0 and 200 m in Table 2 for PFZ and AZ and open ocean (i.e. bathymetry >1000 m) vs stations close to Subantarctic islands (i.e. bathymetry <1000 m). We use BSi:Fuco mass ratios (Fig. 8c) as indicators of the Si:C elemental ratios of diatoms. Si:C was usually found to be higher for diatoms in Fe-depleted areas compared to Fe-repleted areas, which has been attributed to higher diatom silicification (Takeda, 1998; Mosseri et al., 2008; Baines et al., 2010). However, recent studies pointed out that Si:C ratios are mainly driven by the taxonomic composition of the diatom community rather than a short response to iron fertilization (Closset et al., 2014; Lasbleiz et al., 2014; Lafond et al., 2020).

#### 4.3.2. The polar frontal zone

Integrated BSi in the PFZ from our study are higher than those measured during the BONUS GH cruise which was not under any influence from Subantarctic islands, and lower than those measured on the KEOPS2 and MOBYDICK cruises (Table 2) which included stations close to the Kerguelen Plateau where heavily silicified diatom species such as *Fragilariopsis sp.* have been reported (Lasbleiz et al., 2014; Lafond et al., 2020). Indeed, most of the SWINGS PFZ stations are located west of Kerguelen where relative contribution of diatoms to the phytoplankton community is lower (Seeyave et al., 2007), helping to explain the intermediate integrated BSi at the SWINGS PFZ stations.

A closer look at open ocean PFZ stations close to Subantarctic islands (St. 69-70 north to Kerguelen; St. 33, 34 and 35 around Crozet) are characterised by higher BSi, TChla and fucoxanthin concentrations (Fig. 5 and 6) except for St. 18 to 21 around Prince Edward Island. The higher BSi concentrations are probably due to the island mass effect. Around the Subantarctic islands, there is a persistent supply of micronutrients downstream from the islands that can contribute to phytoplankton productivity and facilitate ephemeral blooms in open ocean regions (Robinson et al., 2016; Baldry et al., 2020). BSi and pigment results (Fig. 5), coupled with satellite observations (Fig. 1c and d), highlight the presence of this pattern. However, BSi is not a good tracer as pigments of diatom blooms induced by island mass effects, because BSi is affected both by micronutrient availability modifying Si:C ratios and diatom abundance. This is why BSi:Fuco ratios help in understanding phytoplankton community structure in such patterns, since we expect higher BSi:Fuco ratios under limitation of diatoms primary production.

Integrated BSi:Fuco ratios (Fig. 8c) clearly highlight the stations that might have experienced micronutrient fertilization. All stations around and downstream of Crozet until St.38 have BSi:Fuco ratios <200 while the southernmost stations of the PFZ (31 and 40) have much higher BSi: Fuco ratios (491–534). Stations around the Prince Edward Islands (St. 19–23) have intermediate integrated BSi:Fuco ratios (200–360) that probably result from limited micronutrient fertilization due to the small size of the islands and associated plateau. Finally, the stations to the northeast of the Kerguelen Islands have high BSi concentrations (St. 69, 70; Fig. 6) likely under the influence of the north-western Kerguelen bloom (Fig. 1d, pigment data not available). Recent studies highlight the importance of inputs resulting from glacier melting and weathering, which could bring a significant amount of Fe and Si to the ocean

Table 2 Integrated BSi concentrations ( $\int$  BSi, mmol m<sup>-2</sup>) in the Polar Frontal Zone and the Antarctic Zone from SWINGS and previous cruises in the Southern Ocean. Data have been integrated between 0 and 200 m, except for the WC-17 cruise (82–150 m) and SWINGS PFZ Subantarctic island (0–131 m). Values of integrated BSi correspond to: mean  $\pm$  standard deviation if number of stations visited is  $\geq$ 3; mean (range) if number of stations visited is = 2; value if number of stations visited is = 1. The category "Subantarctic islands" is based on bathymetry <1000 m only, i.e. not based on micronutrient fertilization that can extend further. Bold values were computed using ISP data. The A3 reference station established during the KEOPS program (Blain et al., 2008) is referred as M2 for the MOBYDICK cruise and as St. 68 for the SWINGS cruise. Stations 26 to 29 were classified in the cruise section "SWINGS \*\*\*" apart from the rest of the SWINGS stations, to better highlight the influence of atmospheric inputs at these stations (see section 4.2.1).

Cruise	Season	Sector	$\int$ BSi in PFZ [mmol m <sup>-2</sup> ]		$\int$ BSi in AZ [mmol m <sup>-2</sup> ]			References	
(year)	(period)		Open ocean	Subant. islands	Open ocean	Subant. islands	A3 Station		
KEOPS (2005)	Summer (01/19–02/13)	Indian	-	-	$392\pm131$	$781 \pm 473$	$1111\pm608$	Mosseri et al. (2008)	
BONUS GH (2008)	Late Summer (02/08–03/08)	Atlantic	38 (37–38)		81 ± 29	-	-	Fripiat et al. (2012)	
KEOPS2 (2011)	Spring (10/10–11/20)	Indian	$185\pm130$	-	$245\pm119$	$401\pm197$	452 (164–741)	Lasbleiz et al. (2014); Closset et al. (2016)	
WC-17 (2017)	Winter (06/28-07/13)	Indian	21	-	$52\pm42$	-	-	Weir et al. (2020)	
MOBYDICK (2018)	Late Summer (02/26–16/03)	Indian	166 (139–193)	-	$319\pm175$	$192\pm23$	$192\pm23$	Lafond et al. (2020)	
SWINGS (2021)	Late Summer (01/11–03/08)	Indian	$82\pm49$	58	$206 \pm 90$	$250\pm65$	183	This study	
SWINGS *** (2021)			407 (369–443)	-	701	-	-	This study	

PFZ = Polar Frontal Zone; AZ = Antarctic Zone; Subant. islands = Subantarctic islands.

(Hawkings et al., 2017; van der Merwe et al., 2019), and it is known that the Kerguelen Cook Ice Cap is currently melting at a fast rate mostly on the northern part of the island (Verfaillie et al., 2021).

#### 4.3.3. The Antarctic zone

4.3.3.1. Comparison with previous cruises. Integrated BSi contents describe well the biogeochemical contrasts between two station types (Table 2 and Fig. 8a), where stations above the Kerguelen Plateau benefit from natural micronutrient fertilization with less limitation for diatom growth than at stations far removed from the island influence. These differences were also observed during KEOPS and KEOPS2 cruises with higher integrated BSi compared to our study (Table 2). For KEOPS, Mosseri et al. (2008) emphasized that the bloom during the austral summer of 2005 was unusually intense and almost exclusively composed of large diatoms (Armand et al., 2008). KEOPS2 took place in spring when bloom intensity is always stronger (Closset et al., 2014). Only BSi from the MOBYDICK cruise shows open ocean integrated BSi higher than those above the Kerguelen Plateau, yet it shares the same season as the SWINGS cruise. Lafond et al. (2020) suggest that such high BSi concentrations were due to heavily silicified diatom species particularly abundant at HNLC stations. This leads to integrated BSi values exceeding those above the Kerguelen Plateau, as its seasonal bloom declines during the late austral summer. Overall, this highlights the large interannual variability of BSi in the HNLC waters in the vicinity of the Kerguelen Plateau.

4.3.3.2. Focus on St. 68: A3 reference station (Kerguelen plateau). Above the Kerguelen Plateau, St. 68 corresponds to the St. A3 of KEOPS, KEOPS2 and MOBYDICK (Table 2). The integrated BSi from the SWINGS cruise is in the same range as reported during MOBYDICK. By comparison, the integrated BSi range during KEOPS and KEOPS2 was much higher and as described above, the KEOPS bloom intensity was unusually high while KEOPS2 was sampled during early spring consistent with a decrease of integrated BSi at A3 throughout the season. The structure of the diatom community evolves throughout the growing season where heavily silicified species that can drive BSi towards high values (Armand et al., 2008; Lafond et al., 2020) such as Eucampia antarctica, are replaced by lightly silicified diatoms such as Corethron inerme, Chaetoceros spp. and their resting spores (Lafond et al., 2020). We clearly identified E. antarctica frustules both below the mixed layer at 120 m and at the bottom, whereas no evident Chaetoceros spp. frustules were observed except one resting spore at the bottom (Fig. S4). Therefore, St. 68 was probably sampled before the late austral summer diatom community shift.

4.3.3.3. Focus on St. 29 and St. 58: Unusual high BSi fuelled by distinct processes. Two open ocean stations in the AZ showed intriguing results. First, St. 29 displays a BSi peak of 5.3 μmol L<sup>-1</sup>, which is 4-fold higher than those measured during BONUS GOODHOPE (Fripiat et al., 2012), and an integrated BSi of 701 mmol.m<sup>-2</sup>, which is 3-fold higher than regular open ocean AZ stations (Table 2). Stations 26 and 27 in the PFZ also shared this distinctive feature (Table 2) and form with St. 29 a small transect of higher integrated BSi and LSi (Fig. 8). This difference might be explained by atmospheric inputs measured from St. 26 to 29 as already pointed out in section 4.2.1. Such aerosols, which were not sampled during the BONUS GOODHOPE cruise, are known as a micronutrients source to trigger a phytoplanktonic response in HNLC areas (Mahowald et al., 2009) especially for diatoms (Geisen et al., 2022).

Second, St. 58 which is the southernmost and easternmost stations of SWINGS displayed very high BSi values, reaching 3.7 and 9.1  $\mu mol~L^{-1}$  respectively for NSK and ISP sampling (Fig. 3, 5 and 6). Moreover, SEM observations highlight the very diverse and fresh diatom community, compared to other stations (Fig. S2). These elevated concentrations might be explained by the Antarctic divergence upwelling which could

have brought Si(OH)<sub>4</sub> to the surface as seen from shoaling of Si(OH)<sub>4</sub> concentrations at St. 58 (Fig. S3) and possibly other nutrients, fuelling a late summer/early autumn bloom.

4.3.3.4. Biogenic silica and pigments. Open ocean BSi:Fuco ratios are not significantly different from those above the Kerguelen Plateau (Kruskal-Wallis test, p-value = 0.52). However, two groups of stations above the Kerguelen Plateau can be discriminated (Fig. 8c). St. 45, 46 and 65 close to Heard and MacDonald Islands display high integrated BSi:Fuco ratios (840–1040) despite having a naturally Fe-fertilized character. This is probably due to intense mixing near the Subantarctic islands during SWINGS sampling, as SEM observations revealed the significance of highly fragmented frustules (Fig. S2j) so that the contribution of living diatoms is minor. St. 44, 66 and 68 are stations relatively away from the islands but still above the Kerguelen Plateau with low integrated BSi: Fuco ratios (80–230) caused by relatively high pigment concentrations (Fig. 6) which is in accordance with diatoms bloom.

#### 5. Conclusion

Over the whole SWINGS transect, our results showed that the spatial distribution of BSi was impacted both by the surface water characteristics constrained by the ACC fronts and by an ensemble of contrasting regions. SEM observations on selected samples showed that diatoms were always the dominant siliceous phytoplankton community and therefore likely the most representative of the carrying phase of BSi. Coupled with pigment measurements, BSi results highlighted the contrasts between the HNLC open ocean areas and the naturally fertilized regions close to Subantarctic islands. HNLC open ocean stations were characterised by variable sizes of diatoms and biogenic particles and high BSi:Fuco ratios due to heavily silicified diatoms and/or to the micronutrient limitation. Naturally fertilized regions close to the Subantarctic islands were characterised by the dominance of small biogenic particles, either small and fresh diatoms leading to low BSi:Fuco ratios, or fragmented diatom frustules due to intense water mixing close to the shore and leading to high BSi:Fuco ratios. Overall, size-fractioned results showed that the BSi fraction 0.45–5  $\mu m$  contributes to 47  $\pm$  23% of the total BSi pool in the upper 200 m, mostly as diatom frustule fragments and occasionally small diatoms and Chrysophyceae. We also show that some open ocean stations can have high BSi contents likely due to three different modes of fertilization: aerosol inputs, upwelling or advection when they are downstream of islands. Second, our results showed that LSi is a good tracer of the different lithogenic materials which can be found over the whole SWINGS transect, whether they had a distant wind-driven origin or came from the Subantarctic islands. SEM observations coupled with elemental chemical analyses allowed us to identify a basaltic geochemical composition of LSi in the Kerguelen Plateau region, typical of the geological environments of the islands. In addition, volcanic ashes around Heard and MacDonald Islands are also contributing to the lithogenic particles. Finally, BSi and LSi reproducibility results from two distinct methods using the lithogenic correction by Al confirmed that the initial method proposed by Ragueneau et al. (2005) is more suitable to better correct the BSi concentrations from LSi dissolution, as the study area was prone to diverse continental and volcanic influences whose composition fluctuates. This protocol led to a satisfactory reproducibility of  $13 \pm 7\%$  for BSi  $> 1 \mu mol L^{-1}$ , which is in the same range of the one reported by Ragueneau et al. (2005) for equivalent samples. In addition, having verified the good reproducibility of both Ragueneau et al. (2005) and average crustal ratio methods validates the comparison with previous studies reporting BSi data acquired from different chemical leaching methods. However, for most open ocean Niskin samples, Al concentrations below detection limits precludes lithogenic correction for BSi concentrations.

Our BSi and LSi data bring new information for understanding the marine biogeochemical Si cycle in the South Indian Ocean and Southern

Ocean. In future work, these data will be combined with dissolved and particulate (i.e. biogenic) Si isotopes ( $\delta^{30}$ Si<sub>DSi</sub> and  $\delta^{30}$ Si<sub>BSi</sub>) to better understand the marine biogeochemical Si cycle in the region (Closset et al., 2016). These data can also be coupled with the  $^{234}$ Th flux method where the BSi will enable estimation of BSi export fluxes (Cao et al., 2020) for a better understanding of the functioning of export within the biological carbon pump.

#### CRediT authorship contribution statement

Valentin Deteix: Writing – original draft, Visualization, Validation, Methodology, Formal analysis. Edwin Cotard: Writing – review & editing, Supervision, Methodology, Investigation. Sandrine Caquineau: Writing – review & editing, Supervision, Methodology. William M. Landing: Writing – review & editing, Investigation. Frédéric Planchon: Writing – review & editing, Investigation, Conceptualization. Thomas Ryan-Keogh: Writing – review & editing, Investigation. Damien Cardinal: Writing – review & editing, Supervision, Project administration, Methodology, Investigation, Conceptualization.

#### Declaration of competing interest

The authors declare that the research was conducted in the absence of any commercial or financial relationships that could be construed as a potential conflict of interest.

# Data availability

All BSi and LSi data from either ISP, ISP-SF or NSK, and all total chlorophyll a and fucoxanthin pigments data are available in the SEA-NOE database via the following address: https://doi.org/10.17882/97947.

#### Acknowledgements

The authors would like to thank Catherine Jeandel and Hélène Planquette as the SWINGS chief scientists; the captain and the crew of the R/V "Marion Dufresne II" for assistance on board as well as Marine Piéjus for sampling and filtering on-board; Mustapha Benrahmoune (LOCEAN) for managing clean laboratory; Pierre Burckel and the PARI analytical platform (IPGP) for the Al concentrations measurements: Céline Dimier and the SAPIGH analytical platform (IMEV) for the pigment sample processing and measurements; the Alysés analytical platform (IRD-SU) for the scanning electron microscope observations; Catherine Schmechtig and the LEFE-CYBER Database for data accessibility of previous oceanographic missions. The SWINGS program was supported by the French Research program of INSU-CNRS LEFE-CYBER (Les Enveloppes Fluides de l'Environnement – Cycles biogéochimiques, environnement et ressources) and the French ANR (Agence Nationale de la Recherche, ANR-19-01CE-0012). The authors also thank the two anonymous reviewers for providing constructive and relevant comments on the manuscript. This work was part of the Master's degree research of V. Deteix.

#### Appendix A. Supplementary data

Supplementary data to this article can be found online at https://doi.org/10.1016/j.marchem.2024.104412.

#### References

Armand, L.K., Cornet-Barthaux, V., Mosseri, J., Quéguiner, B., 2008. Late summer diatom biomass and community structure on and around the naturally iron-fertilised Kerguelen plateau in the Southern Ocean. Deep-Sea Res. II Top. Stud. Oceanogr. 55, 653–676. https://doi.org/10.1016/j.dsr2.2007.12.031.

- Baines, S.B., Twining, B.S., Brzezinski, M.A., Krause, J.W., Vogt, S., Assael, D., McDaniel, H., 2012. Significant silicon accumulation by marine picocyanobacteria. Nature Geosci 5, 886–891. https://doi.org/10.1038/ngeo1641.
- Baines, S.B., Twining, B.S., Brzezinski, M.A., Nelson, D.M., Fisher, N.S., 2010. Causes and biogeochemical implications of regional differences in silicification of marine diatoms. Global Biogeochem. Cycles 24. https://doi.org/10.1029/2010GB003856.
- Baldry, K., Strutton, P.G., Hill, N.A., Boyd, P.W., 2020. Subsurface chlorophyll-a maxima in the Southern Ocean. Frontiers in marine. Science 7
- Blain, S., B. Quéguiner, L. Armand, and others. 2007. Effect of natural iron fertilization on carbon sequestration in the Southern Ocean. Nature 446: 1070–1074. doi:https:// doi.org/10.1038/nature05700.
- Blain, S., Quéguiner, B., Trull, T., 2008. The natural iron fertilization experiment KEOPS (KErguelen Ocean and plateau compared study): an overview. Deep-Sea Res. II Top. Stud. Oceanogr. 55, 559–565. https://doi.org/10.1016/j.dsr2.2008.01.002.
- Blain, S., Planquette, H., Obernosterer, I., Guéneuguès, A., 2022. Vertical flux of trace elements associated with Lithogenic and biogenic carrier phases in the Southern Ocean. Glob. Biogeochem. Cycles 36. https://doi.org/10.1029/2022GB007371 e2022GB007371.
- Borchers, A., Voigt, I., Kuhn, G., Diekmann, B., 2011. Mineralogy of glaciomarine sediments from the Prydz Bay–Kerguelen region: relation to modern depositional environments. Antarct. Sci. 23, 164–179. https://doi.org/10.1017/ S0954102010000830.
- Brzezinski, M.A., Nelson, D.M., 1989. Seasonal changes in the silicon cycle within a Gulf Stream warm-core ring. Deep Sea Research Part A. Oceanographic Research Papers 36, 1009–1030. https://doi.org/10.1016/0198-0149(89)90075-7.
- Brzezinski, M.A., Nelson, D.M., 1995. The annual silica cycle in the Sargasso Sea near Bermuda. Deep-Sea Res. I Oceanogr. Res. Pap. 42, 1215–1237. https://doi.org/10.1016/0967-0637(95)93592-3.
- Cao, Z., Wang, D., Zhang, Z., others, 2020. Seasonal dynamics and export of biogenic silica in the upper water column of a large marginal sea, the northern South China Sea. Prog. Oceanogr. 188, 102421 https://doi.org/10.1016/j.pocean.2020.102421.
- Cardinal, D., Dehairs, F., Cattaldo, T., André, L., 2001. Geochemistry of suspended particles in the Subantarctic and polar frontal zones south of Australia: constraints on export and advection processes. J. Geophys. Res. Oceans 106, 31637–31656. https://doi.org/10.1029/2000JC000251.
- Cheize, M., H. F. Planquette, J. N. Fitzsimmons, and others. 2019. Contribution of resuspended sedimentary particles to dissolved iron and manganese in the ocean: an experimental study. Chem. Geol. 511: 389–415. doi:https://doi.org/10.1016/j.ch emgeo.2018.10.003.
- Clements, D.J., Yang, S., Weber, T., McDonnell, A.M.P., Kiko, R., Stemmann, L., Bianchi, D., 2023. New estimate of organic carbon export from optical measurements reveals the role of particle size distribution and export horizon. Glob. Biogeochem. Cycles 37. https://doi.org/10.1029/2022GB007633 e2022GB007633.
- Closset, I., Lasbleiz, M., Leblanc, K., Quéguiner, B., Cavagna, A.-J., Elskens, M., Navez, J., Cardinal, D., 2014. Seasonal evolution of net and regenerated silica production around a natural Fe-fertilized area in the Southern Ocean estimated with Si isotopic approaches. Biogeosciences 11, 5827–5846. https://doi.org/10.5194/bg-11-5827-2014
- Closset, I., D. Cardinal, M. Rembauville, F. Thil, and S. Blain. 2016. Unveiling the Si cycle using isotopes in an iron fertilized zone of the Southern Ocean: from mixed layer supply to export. Preprint biogeochemistry: Open Ocean.
- DeVries, T., Weber, T., 2017. The export and fate of organic matter in the ocean: new constraints from combining satellite and oceanographic tracer observations. Glob. Biogeochem. Cycles 31, 535–555. https://doi.org/10.1002/2016GB005551.
- Dugdale, R.C., Wilkerson, F.P., Minas, H.J., 1995. The role of a silicate pump in driving new production. Deep-Sea Res. I Oceanogr. Res. Pap. 42, 697–719. https://doi.org/ 10.1016/0967-0637(95)00015-X.
- Efstathiou, C.E., 2006. Estimation of type I error probability from experimental Dixon's "Q" parameter on testing for outliers within small size data sets. Talanta 69, 1068–1071. https://doi.org/10.1016/j.talanta.2005.12.031.
- Eggimann, D.W., Betzer, P.R., 1976. Decomposition and analysis of refractory oceanic suspended materials. Anal. Chem. 48, 886–890. https://doi.org/10.1021/ ac60370a005.
- Field, C.B., Behrenfeld, M.J., Randerson, J.T., Falkowski, P., 1998. Primary production of the biosphere: integrating terrestrial and oceanic components. Science 281, 237–240. https://doi.org/10.1126/science.281.5374.237.
- Fox, J.M., McPhie, J., Carey, R.J., Jourdan, F., Miggins, D.P., 2021. Construction of an intraplate island volcano: the volcanic history of heard island. Bull. Volcanol. 83, 37. https://doi.org/10.1007/s00445-021-01452-5.
- Fripiat, F., Cavagna, A.-J., Savoye, N., Dehairs, F., André, L., Cardinal, D., 2011. Isotopic constraints on the Si-biogeochemical cycle of the Antarctic zone in the Kerguelen area (KEOPS). Mar. Chem. 123, 11–22. https://doi.org/10.1016/j. marchem.2010.08.005.
- Franck, V., Brzezinski, M.A., Coale, K.H., Nelson, D.M., 2000. Iron and silicic acid concentrations regulate Si uptake north and south of the Polar Frontal Zone in the Pacific Sector of the Southern Ocean. Deep Sea Research Part II. Topical Studies in Oceanography, US Southern Ocean JGOFS Program (AESOPS) 47, 3315–3338. https://doi.org/10.1016/S0967-0645(00)00070-9.
- Fripiat, F., Cavagna, A.-J., Dehairs, F., de Brauwere, A., André, L., Cardinal, D., 2012. Processes controlling the Si-isotopic composition in the Southern Ocean and application for paleoceanography. Biogeosciences 9, 2443–2457. https://doi.org/ 10.5194/bg-9-2443-2012.
- Gehlen, M., Beck, L., Calas, G., Flank, A.-M., Van Bennekom, A.J., Van Beusekom, J.E.E., 2002. Unraveling the atomic structure of biogenic silica: evidence of the structural association of Al and Si in diatom frustules. Geochim. Cosmochim. Acta 66, 1601–1609. https://doi.org/10.1016/S0016-7037(01)00877-8.

- Geisen, C., C. Ridame, E. Journet, and others. 2022. Phytoplanktonic response to simulated volcanic and desert dust deposition events in the south Indian and southern oceans. Limnol. Oceanogr. 67: 1537–1553. doi:https://doi.org/10.1002/ lno.12100.
- Grasshoff, K., Kremling, K., Ehrhardt, M., 2009. Methods of Seawater Analysis. John Wiley & Sons.
- Gruber, N., Landschützer, P., Lovenduski, N.S., 2019. The variable Southern Ocean carbon sink. Annu. Rev. Mar. Sci. 11, 159–186. https://doi.org/10.1146/annurevmarine-121916-063407.
- Hawkings, J.R., Wadham, J.L., Benning, L.G., Hendry, K.R., Tranter, M., Tedstone, A., Nienow, P., Raiswell, R., 2017. Ice sheets as a missing source of silica to the polar oceans. Nat. Commun. 8, 14198. https://doi.org/10.1038/ncomms14198.
- Henson, S.A., Sanders, R., Madsen, E., Morris, P.J., Le Moigne, F., Quartly, G.D., 2011.
  A reduced estimate of the strength of the ocean's biological carbon pump. Geophys.
  Res. Lett. 38 https://doi.org/10.1029/2011GL046735.
- Holzer, M., Primeau, F.W., DeVries, T., Matear, R., 2014. The Southern Ocean silicon trap: data-constrained estimates of regenerated silicic acid, trapping efficiencies, and global transport paths. J. Geophys. Res. Oceans 119, 313–331. https://doi.org/10.1002/2013.0009356
- Jeandel, C., Ruiz-Pino, D., Gjata, E., others, 1998. KERFIX, a time-series station in the Southern Ocean: a presentation. J. Mar. Syst. 17, 555–569. https://doi.org/10.1016/ S0924-7963(98)00064-5.
- Krause, J.W., Lomas, M.W., Danielson, S.L., 2021. Diatom growth, biogenic silica production, and grazing losses to microzooplankton during spring in the northern Bering and Chukchi Seas. Deep Sea Research Part II. Topical Studies in Oceanography 191–192, 104950. https://doi.org/10.1016/j.dsr2.2021.104950.
- Lafond, A., Leblanc, K., Legras, J., Cornet, V., Quéguiner, B., 2020. The structure of diatom communities constrains biogeochemical properties in surface waters of the Southern Ocean (Kerguelen plateau). J. Mar. Syst. 212, 103458 https://doi.org/ 10.1016/j.imarsys.2020.103458.
- Lamont, T., Tutt, G.C.O., Barlow, R.G., 2022. Phytoplankton biomass and photophysiology at the sub-Antarctic Prince Edward islands ecosystem in the Southern Ocean. J. Mar. Syst. 226, 103669 https://doi.org/10.1016/j. jmarsys.2021.103669.
- Lasbleiz, M., Leblanc, K., Blain, S., Ras, J., Cornet-Barthaux, V., Hélias Nunige, S., Quéguiner, B., 2014. Pigments, elemental composition (C, N, P, and Si), and stoichiometry of particulate matter in the naturally iron fertilized region of Kerguelen in the Southern Ocean. Biogeosciences 11, 5931–5955. https://doi.org/ 10.5194/be-11-5931-2014.
- Le Moigne, F.A.C., 2019. Pathways of organic carbon downward transport by the oceanic biological carbon pump. Frontiers in marine. Science 6.
- Leblanc, K., Quéguiner, B., Fiala, M., Blain, S., Morvan, J., Corvaisier, R., 2002.
  Particulate biogenic silica and carbon production rates and particulate matter distribution in the Indian sector of the Subantarctic Ocean. Deep-Sea Res. II Top. Stud. Oceanogr. 49, 3189–3206. https://doi.org/10.1016/S0967-0645(02)00078-4.
- Li, F., Ginoux, P., Ramaswamy, V., 2008. Distribution, transport, and deposition of mineral dust in the Southern Ocean and Antarctica: contribution of major sources. J. Geophys. Res. Atmos. 113 https://doi.org/10.1029/2007JD009190.
- Mahowald, N. M., S. Engelstaedter, C. Luo, and others. 2009. Atmospheric Iron deposition: global distribution, variability, and human perturbations. Annu. Rev. Mar. Sci. 1: 245–278. doi:https://doi.org/10.1146/annurev.marine.010908.163727.
- Martin, J.H., 1990. Glacial-interglacial CO2 change: the Iron hypothesis. Paleoceanography 5, 1–13. https://doi.org/10.1029/PA005i001p00001.
- McCave, I. N. 2009. Nepheloid layers, p. 8–18. In J.H. Steele [ed.], encyclopedia of ocean sciences (second edition). Academic press.
- Mosseri, J., Quéguiner, B., Armand, L., Cornet-Barthaux, V., 2008. Impact of iron on silicon utilization by diatoms in the Southern Ocean: a case study of Si/N cycle decoupling in a naturally iron-enriched area. Deep-Sea Res. II Top. Stud. Oceanogr. 55, 801–819. https://doi.org/10.1016/j.dsr2.2007.12.003.
- Murray, R.W., Leinen, M., Isern, A.R., 1993. Biogenic flux of Al to sediment in the central equatorial Pacific Ocean: evidence for increased productivity during glacial periods. Paleoceanography 8, 651–670. https://doi.org/10.1029/93PA02195.
- Nelson, D.M., W. O. Smith Jr., 1991. Sverdrup revisited: critical depths, maximum chlorophyll levels, and the control of Southern Ocean productivity by the irradiancemixing regime. Limnol. Oceanogr. 36, 1650–1661. https://doi.org/10.4319/ lo.1991.36.8.1650.
- Nelson, D.M., Brzezinski, M.A., Sigmon, D.E., Franck, V.M., 2001. A seasonal progression of Si limitation in the Pacific sector of the Southern Ocean. Deep-Sea Res. II Top. Stud. Oceanogr. 48, 3973–3995. https://doi.org/10.1016/S0967-0645(01)00076-5.
- Nissen, C., Gruber, N., Münnich, M., Vogt, M., 2021. Southern Ocean phytoplankton community structure as a gatekeeper for global nutrient biogeochemistry. Glob. Biogeochem. Cycles 35. https://doi.org/10.1029/2021GB006991 e2021GB006991.
- Park, Y.-H., Roquet, F., Durand, I., Fuda, J.-L., 2008. Large-scale circulation over and around the northern Kerguelen plateau. Deep-Sea Res. II Top. Stud. Oceanogr. 55, 566–581. https://doi.org/10.1016/j.dsr2.2007.12.030.
- Pollard, R. T., I. Salter, R. J. Sanders, and others. 2009. Southern Ocean deep-water carbon export enhanced by natural iron fertilization. Nature 457: 577–580. doi: https://doi.org/10.1038/nature07716.

- Quéguiner, B., 2001. Biogenic silica production in the Australian sector of the Subantarctic zone of the Southern Ocean in late summer 1998. J. Geophys. Res. Oceans 106, 31627–31636. https://doi.org/10.1029/2000JC000249.
- Quéguiner, B., Tréguer, P., Peeken, I., Scharek, R., 1997. Biogeochemical dynamics and the silicon cycle in the Atlantic sector of the Southern Ocean during austral spring 1992. Deep-Sea Res. II Top. Stud. Oceanogr. 44, 69–89. https://doi.org/10.1016/ S0967-0645(96)00066-5.
- Quilty, P.G., Wheller, G.E., 2000. Heard island and the McDonald Islands: a window into the Kerguelen plateau. Pap. Proc. R. Soc. Tasmania 133, 1–12. https://doi.org/10.26749/rstpp.133.2.1.
- Ragueneau, O., Savoye, N., Del Amo, Y., Cotten, J., Tardiveau, B., Leynaert, A., 2005.
  A new method for the measurement of biogenic silica in suspended matter of coastal waters: using Si:Al ratios to correct for the mineral interference. Cont. Shelf Res. 25, 697–710. https://doi.org/10.1016/j.csr.2004.09.017.
- Ras, J., Claustre, H., Uitz, J., 2008. Spatial variability of phytoplankton pigment distributions in the subtropical South Pacific Ocean: comparison between in situ and predicted data. Biogeosciences 5, 353–369. https://doi.org/10.5194/bg-5-353-2008
- Regard, V., M. Prémaillon, T. J. B. Dewez, and others. 2022. Rock coast erosion: an overlooked source of sediments to the ocean. Europe as an example. Earth Planet. Sci. Lett. 579: 117356. doi:https://doi.org/10.1016/j.epsl.2021.117356.
- Robinson, J., Popova, E.E., Srokosz, M.A., Yool, A., 2016. A tale of three islands: downstream natural iron fertilization in the Southern Ocean. J. Geophys. Res. Oceans 121, 3350–3371. https://doi.org/10.1002/2015JC011319.
- Sarmiento, J.L., Gruber, N., Brzezinski, M.A., Dunne, J.P., 2004. High-latitude controls of thermocline nutrients and low latitude biological productivity. Nature 427, 56–60. https://doi.org/10.1038/nature02127.
- Schlitzer, Reiner, 2024. Ocean Data View. https://odv.awi.de.
- Sedwick, P.N., Blain, S., Quéguiner, B., Griffiths, F.B., Fiala, M., Bucciarelli, E., Denis, M., 2002. Resource limitation of phytoplankton growth in the Crozet Basin, Subantarctic Southern Ocean. Deep-Sea Res. II Top. Stud. Oceanogr. 49, 3327–3349. https://doi. org/10.1016/S0967-0645(02)00086-3.
- Seeyave, S., Lucas, M.I., Moore, C.M., Poulton, A.J., 2007. Phytoplankton productivity and community structure in the vicinity of the Crozet plateau during austral summer 2004/2005. Deep-Sea Res. II Top. Stud. Oceanogr. 54, 2020–2044. https://doi.org/ 10.1016/j.dsr2.2007.06.010.
- Siegel, D.A., Buesseler, K.O., Doney, S.C., Sailley, S.F., Behrenfeld, M.J., Boyd, P.W., 2014. Global assessment of ocean carbon export by combining satellite observations and food-web models. Glob. Biogeochem. Cycles 28, 181–196. https://doi.org/ 10.1002/2013GB004743.
- Sokolov, S., Rintoul, S.R., 2009. Circumpolar structure and distribution of the Antarctic circumpolar current fronts: 1. Mean circumpolar paths. J. Geophys. Res. Oceans 114. https://doi.org/10.1029/2008JC005108.
- Takeda, S., 1998. Influence of iron availability on nutrient consumption ratio of diatoms in oceanic waters. Nature 393, 774–777. https://doi.org/10.1038/31674.
- Taylor, S.R., McLennan, S.M., 1985. The Continental Crust: Its Composition and Evolution.
- Thi Dieu, Vu, H., and Y. Sohrin., 2013. Diverse stoichiometry of dissolved trace metals in the Indian Ocean. Sci. Rep. 3, 1745. https://doi.org/10.1038/srep01745.
- Tian, Q., D. Liu, P. Yuan, and others. 2022. Occurrence of structural aluminium (Al) in marine diatom biological silica: visible evidence from microscopic analysis. Ocean Sci. 18: 321–329. doi:https://doi.org/10.5194/os-18-321-2022.
- Tréguer, P. J., J. N. Sutton, M. Brzezinski, and others. 2021. Reviews and syntheses: the biogeochemical cycle of silicon in the modern ocean. Biogeosciences 18: 1269–1289. doi:https://doi.org/10.5194/bg-18-1269-2021.
- van Beek, P., Bourquin, M., Reyss, J.-L., Souhaut, M., Charette, M.A., Jeandel, C., 2008. Radium isotopes to investigate the water mass pathways on the Kerguelen plateau (Southern Ocean). Deep-Sea Res. II Top. Stud. Oceanogr. 55, 622–637. https://doi. org/10.1016/j.dsr2.2007.12.025.
- Van Bennekom, A.J., Buma, A.G.J., Nolting, R.F., 1991. Dissolved aluminium in the Weddell-scotia confluence and effect of Al on the dissolution kinetics of biogenic silica. Mar. Chem. 35, 423–434. https://doi.org/10.1016/S0304-4203(09)90034-2.
- van der Merwe, P., K. Wuttig, T. Holmes, T. W. Trull, Z. Chase, A. T. Townsend, K. Goemann, and A. R. Bowie. 2019. High lability Fe particles sourced from glacial Erosion can meet previously unaccounted biological demand: heard island, Southern Ocean. Frontiers in marine science 6.
- Verfaillie, D., Charton, J., Schimmelpfennig, I., others, 2021. Evolution of the cook ice cap (Kerguelen Islands) between the last centuries and 2100 ce based on cosmogenic dating and glacio-climatic modelling. Antarct. Sci. 33, 301–317. https://doi.org/ 10.1017/S0954102021000080.
- Weir, I., Fawcett, S., Smith, S., Walker, D., Bornman, T., Fietz, S., 2020. Winter biogenic silica and diatom distributions in the Indian sector of the Southern Ocean. Deep-Sea Res. I Oceanogr. Res. Pap. 166, 103421 https://doi.org/10.1016/j.dsr.2020.103421.
- Wise Jr., S.W., Schlich, R., et al. (Eds.), 1992. Proceedings of the Ocean Drilling Program, 120 Scientific Results. Ocean Drilling Program.
- Yeghicheyan, D., D. Aubert, M. Bouhnik-Le Coz, and others. 2019. A new Interlaboratory characterisation of silicon, rare earth elements and twenty-two other trace element concentrations in the Natural River water certified reference material SLRS-6 (NRC-CNRC). Geostand. Geoanal. Res. 43: 475–496. doi:https://doi.org/10.1111/ggr 12268